2025 DRAGON 6 SYMPOSIUM

14-18 JULY 2025

PROJECT ID. 95235

EO-AI4ResilientCities: Advancing Urban and Environmental Resilience with AI-Driven Earth Observation







2025 Dragon 6 Symposium

<Day 2 & 15 July 2025>

ID. 95235

PROJECT TITLE: EO-AI4ResilientCities
Advancing Urban and Environmental Resilience with AI-Driven Earth Observation

PRINCIPAL INVESTIGATORS: Yifang Ban & Peijun Du

CO-PIS: Paolo Gamba, Linlin Lu, Kun Tan, Zhen Xu

PRESENTED BY: Yifang Ban, Peijun Du, Linlin Lu, Kun Tan & Zhen Xu

Research Objectives

The overall objective of this project is to enhance urban resilience and sustainability by leveraging EO image time series and state-of-the-art deep learning methods, focusing on urban mapping, urbanization monitoring, environmental resilience assessment, and urban building and infrastructure monitoring and vulnerability evaluation.

Dragon 6 EO Data Delivery

Data access (list all missions and issues if any). NB. in the tables please insert cumulative figures (since June 2024) for no. of scenes of high bit rate data (e.g. S1 100 scenes). If data delivery is low bit rate by ftp, insert “ftp”

ESA /Copernicus Missions	No. Scenes
1. Sentinel-1	2435
2. Sentinel-2	5376
3.	
4.	
5.	
6.	
7.	
Total:	
Issues:	

ESA Third Party Missions	No. Scenes
1. COSMO-SkyMed	4
2. Landsat 5/7/8/9	50
3. NOAA VIIRS TIR	108
4. NOAA VIIRS LST	108
5.	
6.	
7.	
Total:	
Issues:	

Chinese EO data	No. Scenes
1. SDGSAT-1 GIU	382
2. SDGSAT-1 TIS	124
3. GF-2	2
4. JGF-1	3
5. Jinlin-1	10
6. 0.1 meter resolution aerial imagery	Shanghai
7. GF-7	2
Total:	
Issues:	

European Young Scientists contributions in Dragon 6

Name	Institution	Poster title	Contribution including period of research
Eric Brune	KTH Royal Institute of Technology, Sweden	Diffusion Models for Daily High-Resolution Urban Land Surface Temperature (LST) Mapping	Introducing a diffusion model that fuses daily low-resolution Sentinel-3 thermal data with high-resolution SDGSat-1 data to generate high-resolution daily urban LST, effectively bridging the spatiotemporal gap in Urban Heat Islands monitoring. 2025-2027.
Luigi Russo	University of Pavia, Italy	Deep Learning Advancements for Urban Change Detection Using Multitemporal SAR Images from Heterogeneous Sensors	This work presents a SAR-to-SAR deep learning framework based on CycleGANs to improve change detection across heterogeneous SAR sensors (Sentinel-1 and COSMO-SkyMed). The study focuses on synthetic image generation to reduce domain shifts and improve cross-sensor alignment and the detection of changes in urban areas such as Rio de Janeiro and Hong Kong. 2025-2028.

Diffusion Model for Daily High-Resolution Urban Land Surface Temperature (LST) Mapping

Introduction

- The Urban Heat Island (UHI) effect significantly impacts human health, energy demand, and environmental conditions in cities, necessitating precise and frequent monitoring.
- Existing satellite systems face a trade-off between spatial resolution and temporal frequency, e.g, VIIRS provides daily coverage but at coarse resolution (375–750 m), while SDGSAT-1 offers fine detail (30 m) but lacks frequent revisits, limiting their effectiveness for detailed, dynamic UHI analysis.
- Limitations of Current Downscaling Methods: Traditional downscaling techniques fail to preserve critical urban-scale thermal features, hindering localized climate adaptation efforts.

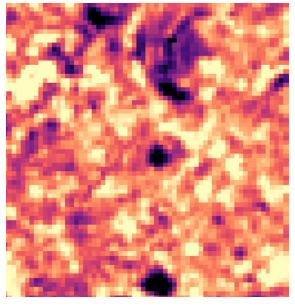
Research Objectives

- To develop a generative-model-based framework that fuses coarse-resolution daily VIIRS data with high-resolution but infrequent SDGSAT-1 imagery to produce daily 30 m Land Surface Temperature maps for improved UHI monitoring and mitigation.

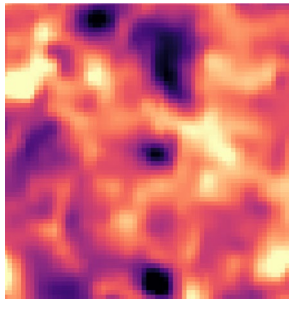
Barcelona city center



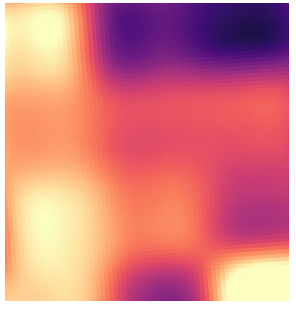
SDGSAT-1 LST



Landsat-8 LST



VIIRS Band I5



Study Areas and Satellite Data

Study Areas

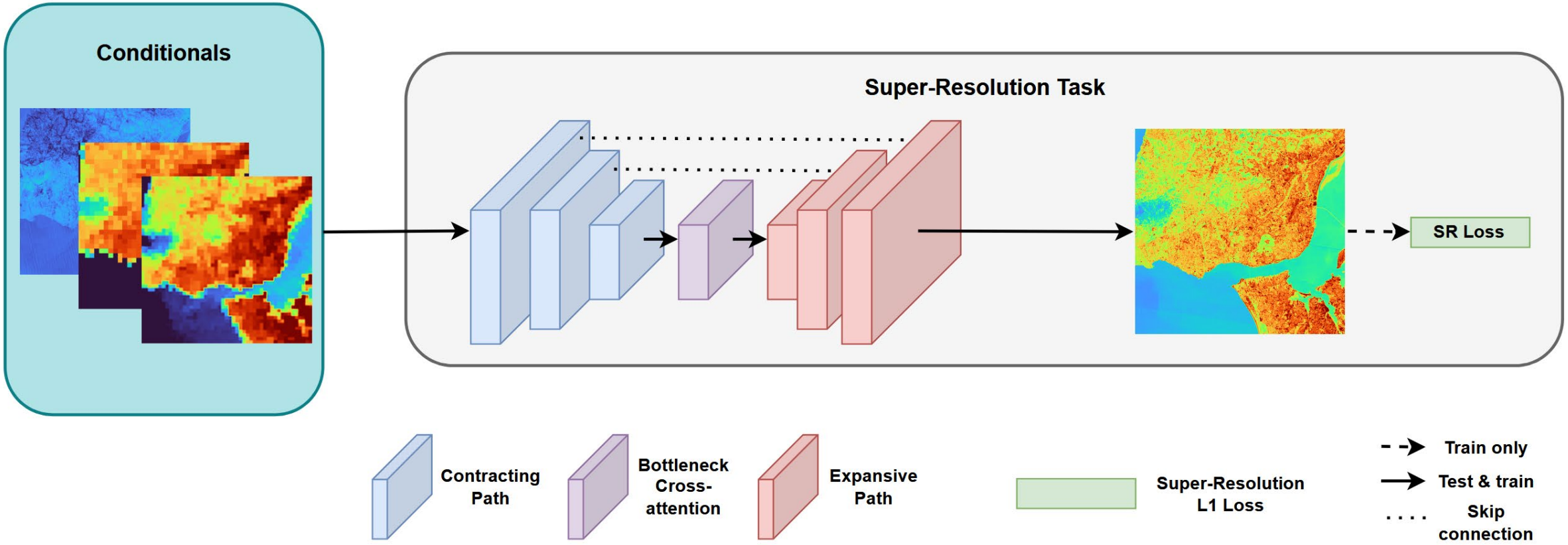
- Eleven major European cities (shown below) were used for training and testing. Each urban footprint is clipped to its city boundaries and projected to its local CRS.

Satellite Data

- VIIRS I5 (11.45 μm) radiance (375 m)
- VIIRS Land Surface Temperature (1000 m)
- SDGSAT-1 TIS channels (8–12.5 μm, 30 m) converted to LST



Methodology: Diffusion-based Super-Resolution



Overview of European YSs research

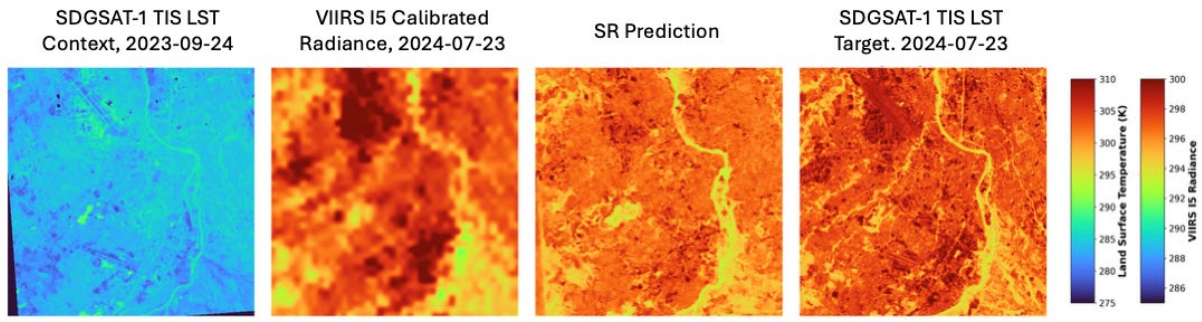
Results & Conclusion

- The SR3-based diffusion model is able to generate daily 30 m LST mosaics for European cities with relatively high accuracy.
- Cities like Rome and Athens showed the best results, while Milan shows the highest error due to limited training data.
- The model accurately reconstructs features like sharp river corridors and urban hotspots that are indistinguishable in 375m data, benefiting from high-resolution LST maps from SDGSAT-1 TIS.
- The model can support daily heat-wave surveillance and near-real-time urban-climate analytics.

City	MAE (K)	RMSE (K)
Athens	1.35	1.63
Barcelona	5.45	6.14
Heraklion	3.7	3.77
Lisbon	5.62	5.89
Madrid	5.96	6.53
Milan	6.9	7.79
Palermo	4.34	4.91
Rome	1.51	1.87
Stockholm	2.56	3.33
Thessaloniki	5.19	5.37
Toulouse	2.57	3.38
Mean	4.10	4.60

Future Research

- Extending the training set, refine the preprocessing of input data, and integrate novel architecture and sampling methods for faster inference.



Overview of European YSs research

"Deep Learning Advancements for Urban Change Detection Using Multitemporal SAR Images from Heterogeneous Sensors"

Introduction:

- **Urbanization** drives global change, demanding **accurate monitoring** for effective **urban planning** and **environmental monitoring**.
- **Synthetic Aperture Radar** (**SAR**) sensors offer **all-weather, day-night imaging**, but working with **heterogeneous sensors** is challenging.
- This study uses a **deep learning (DL) SAR-to-SAR framework** to create **synthetic aligned image pairs**, improving **change detection (CD)** when **co-temporal data** from the same sensor is **unavailable**.

Objective:

- Evaluate a **SAR-to-SAR DL framework** for **CD** using **pre/post-event SAR pairs** from **heterogeneous sensors**.
- Test areas and data: **Rio de Janeiro** and **Hong Kong** (*Table 1*).
- Goal: assess if **synthetic generated SAR pairs** can support the detection of **urban** and **environmental changes.**

City	Sensor	Acquisition Type	Date	Polarization	Imaging Mode
Rio de Janeiro	COSMO-SkyMed	Pre-event	2016-04-18	HH	Stripmap Himage
	Sentinel-1	Pre-event	2016-04-20	VV	Interferometric Wide Swath
	COSMO-SkyMed	Post-event	2017-10-14	HH	Stripmap Himage
	Sentinel-1	Post-event	2017-10-06	VV	Interferometric Wide Swath
Hong Kong	COSMO-SkyMed	Pre-event	2016-08-29	HH	Stripmap Himage
	Sentinel-1	Pre-event	2016-09-25	VV	Interferometric Wide Swath
	COSMO-SkyMed	Post-event	2018-10-22	HH	Stripmap Himage
	Sentinel-1	Post-event	2018-03-19	VV	Interferometric Wide Swath

Table 1: SAR acquisition details for Rio de Janeiro and Hong Kong.

Overview of European YSs research

Phase 1: SAR-to-SAR Translation:

- Use **CycleGAN** with two generators and two discriminators to **translate between SAR domains** : Sentinel-1 (VV) ↔ COSMO-SkyMed (HH).
- Optimize the translation using **adversarial**, **cycle-consistency**, and **identity losses** to generate **realistic and coherent synthetic images**.

Phase 2 – Change Detection:

- **Apply a Siamese U-Net** to compare real and synthetic SAR image pairs and detect **urban changes**.
- The model is optimized using a combination of **Dice Loss** and **Cross-Entropy Loss** for **pixel-level classification**.

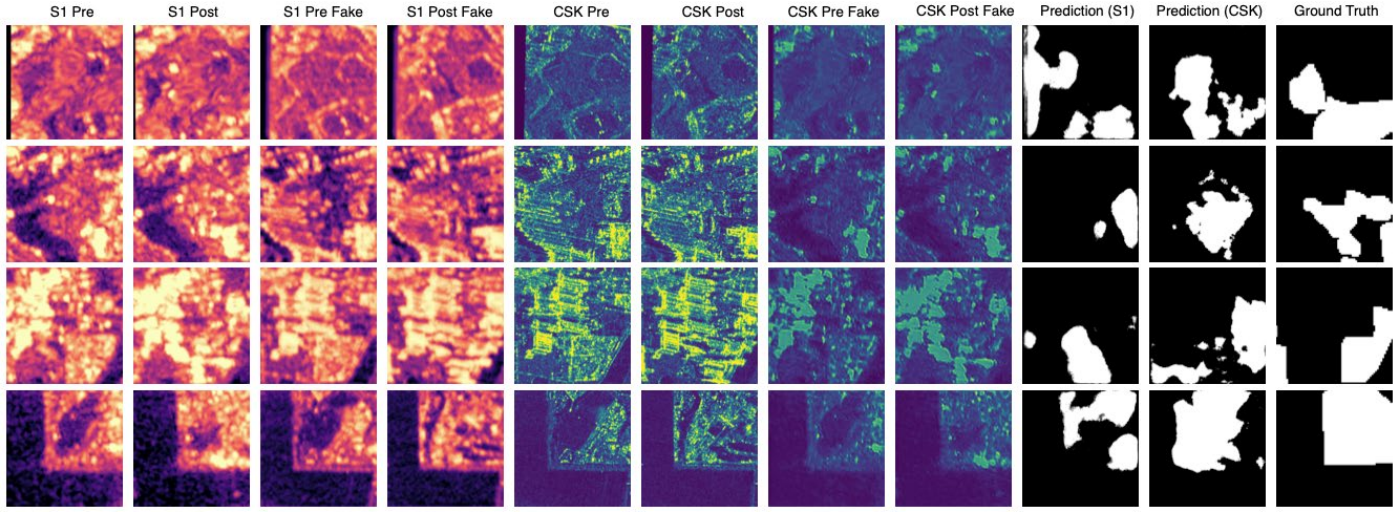
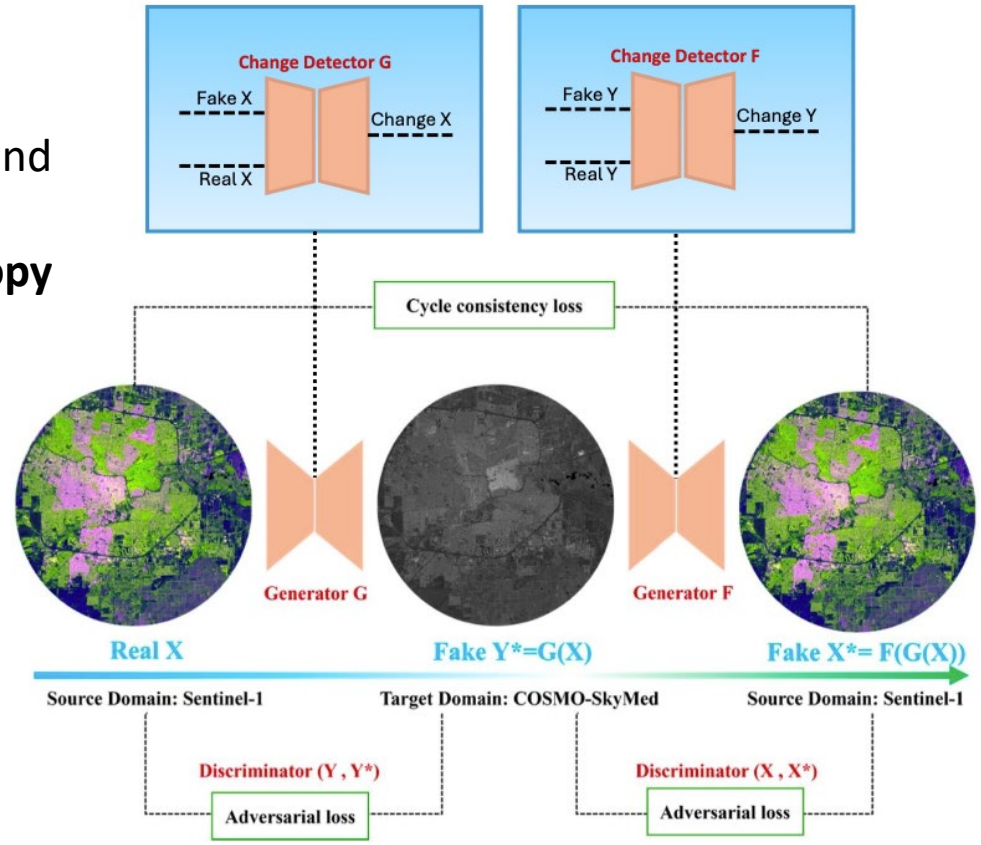


Fig. 1. Qualitative results of the SAR-to-SAR and Change Detection pipeline. From left to right: real and synthetic (fake) pre & post-event SAR patches for Sentinel-1 (S1) and COSMO-SkyMed (CSK), followed by change predictions and GT masks.

Fig. 2. Overview of the proposed framework: a CycleGAN module translates between Sentinel-1 and COSMO-SkyMed domains, while a Change Detection module uses real/synthetic pairs to predict urban change masks.



Overview of European YSs research

Results: SAR-to-SAR Translation

- **Synthetic SAR images** effectively **reduce domain gaps** (↑**SSIM**, ↑**PSNR**, ↓**MSE**, *Table 2*).
- **Limitation: resolution mismatch**.
- **Future work:** extend to **longer sequences** and explore **advanced frameworks** (e.g., **diffusion models**) for enhanced **robustness**.

Results: Change Detection

- **Hybrid pairs** (real + synthetic) outperform direct heterogeneous comparisons.
- In **5-fold cross-validation** (*Table 3*, upper), hybrid pairs improve **IoU by +35–69%**, **F1 by +33–63%**, with slightly lower recall due to fewer false positives.
- In **Out-of-Distribution (OOD) tests** (train: Rio, test: Hong Kong), hybrid inputs still yield **+30–37% IoU** and **~27% F1** gains, showing strong **robustness to domain shift** (Table 4, bottom).
- **Overall, hybrid CD setups consistently outperform heterogeneous baselines** (i.e., direct comparisons between SAR images from different sensors) **in both known and unseen scenarios.**

Comparison	MSE ↓	PSNR ↑	SSIM ↑
Real CSK vs Real S1	0.1156	10.78	0.161
Real CSK vs Fake CSK	**0.0285**	**16.90**	**0.256**
Real S1 vs Fake S1	**0.0377**	**14.71**	**0.378**

Table 2: Similarity metrics for real and SAR-to-SAR-generated image pairs.

Setting	Sensor	Configuration	IoU	F1-Score	Recall
5-fold cross-validation	CSK	Ideal (CSK Pre vs CSK Post)	**0.365 ± 0.049**	**0.533 ± 0.052**	**0.605 ± 0.116**
		Hybrid (CSK Pre Fake vs CSK Post)	**0.086 ± 0.027** (+69%)	**0.158 ± 0.044** (+63%)	0.692 ± 0.055 (–5%)
		Worst-case (S1 Pre vs CSK Post)	0.051 ± 0.016	0.097 ± 0.029	**0.727 ± 0.125**
	S1	Ideal (S1 Pre vs S1 Post)	**0.218 ± 0.033**	**0.357 ± 0.043**	**0.403 ± 0.086**
		Hybrid (S1 Pre Fake vs S1 Post)	**0.088 ± 0.021** (+35%)	**0.161 ± 0.036** (+33%)	0.569 ± 0.070 (–14%)
		Worst-case (CSK Pre vs S1 Post)	0.065 ± 0.020	0.121 ± 0.036	**0.659 ± 0.123**
OOD (Hong Kong)	CSK	Ideal (CSK Pre vs CSK Post)	**0.186**	**0.313**	**0.450**
		Hybrid (CSK Pre Fake vs CSK Post)	**0.070** (+37%)	**0.123** (+27%)	0.675 (–22%)
		Worst-case (S1 Pre vs CSK Post)	0.051	0.097	**0.866**
	S1	Ideal (S1 Pre vs S1 Post)	**0.144**	**0.251**	**0.341**
		Hybrid (S1 Pre Fake vs S1 Post)	**0.060** (+30%)	**0.111** (+26%)	0.583 (–29%)
		Worst-case (CSK Pre vs S1 Post)	0.046	0.088	**0.816**

Table 3: Change detection performance using S1 and CSK inputs. Hybrid configurations leverage SAR-to-SAR translation. The top section shows five-fold cross-validation with mixed training samples from Hong Kong and Rio de Janeiro. The bottom section presents the out-of-distribution (OOD) test on Hong Kong, with training performed on Rio de Janeiro only. Percentage deltas indicate improvement (+) or drop (–) of hybrid setups compared to the worst-case scenario (*i.e.*, comparing pre/post images from heterogeneous SAR sensors).

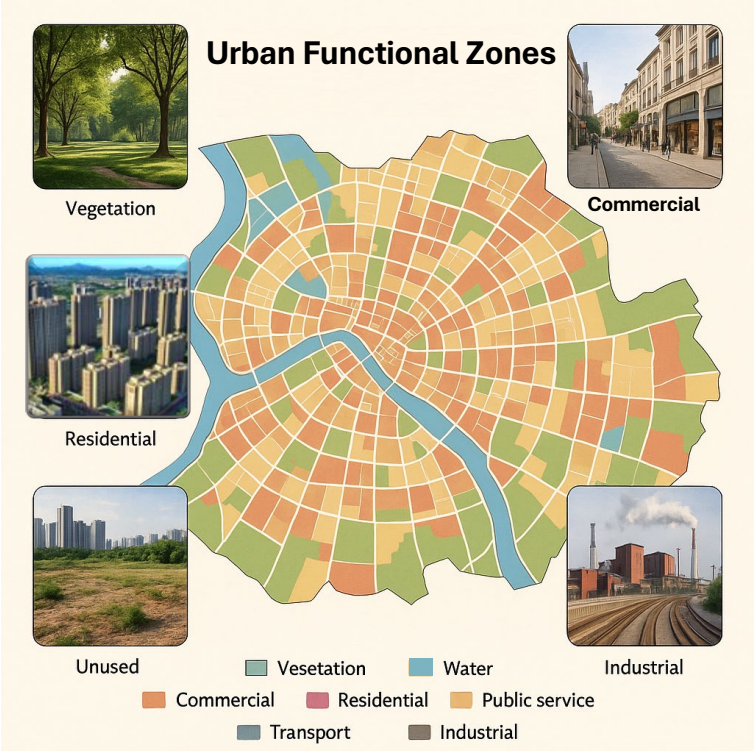
Chinese Young Scientists contributions in Dragon 6

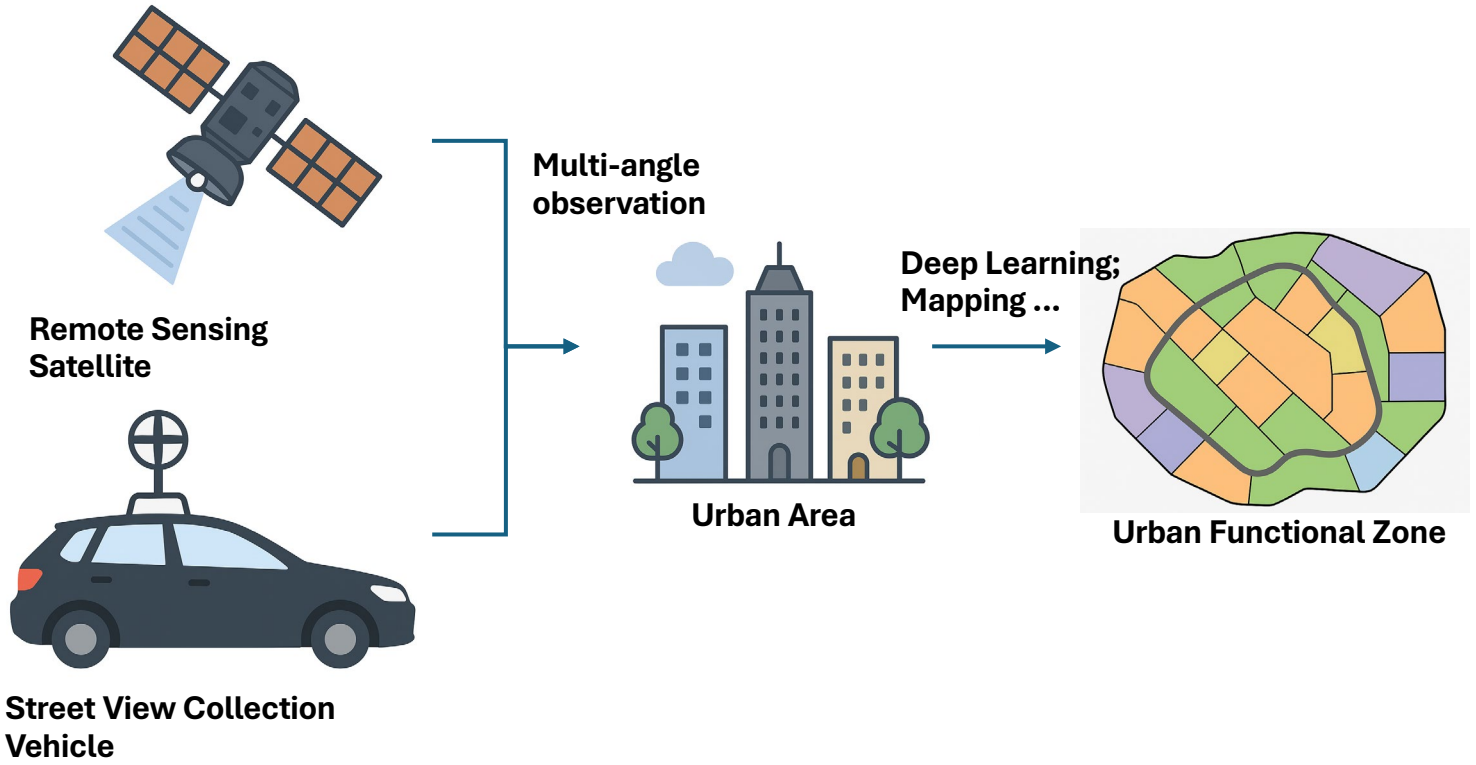
Name	Institution	Poster title	Contribution including period of research
Chenghan Yang	Nanjing University	Urban Functional Zone Change Detection via Multi-Source Temporal Fusion of Street View and Remote Sensing Imagery	Developed a deep learning method (MSTF) for UFZs change detection using multi-temporal Street View and Remote Sensing imagery. 2025-2029
Chunqiang Li	Nanjing University	Dynamic Monitoring of Fine-grained Ecological Vulnerability in Dryland Urban Agglomeration Integrating Novel Remote Sensing Index and Explainable Machine Learning	A novel Dryland Ecological Vulnerability Index (DEVI) is proposed to simplify the traditional complex vulnerability scoping diagram (VSD) and monitor ecological vulnerability changes in arid city clusters from 1986-2024. 2025-2027
Haowei Mu	Nanjing University	Quantifying the Anthropogenic Sensitivity of Ecological Patterns in Arid Urban Agglomeration	Ecological sensitivity to human activities is assessed through a combination of Morphological Spatial Pattern Analysis (MSPA), InVEST habitat quality modeling, and connectivity analysis. 2025-2026

Overview of Chinese YSs research

Advancing Urban Monitoring: Urban Functional Zone Change Detection via Multi-Source Temporal Fusion of Street View and Remote Sensing Imagery

- Urban Functional Zones (UFZ) reflect the refinement of **urban functions** and their spatial heterogeneity, making them crucial for understanding and managing urban development.
- In our study, UFZ dynamics were detected through **multi-source spatiotemporal fusion** of **street view** and **remote sensing** imagery.



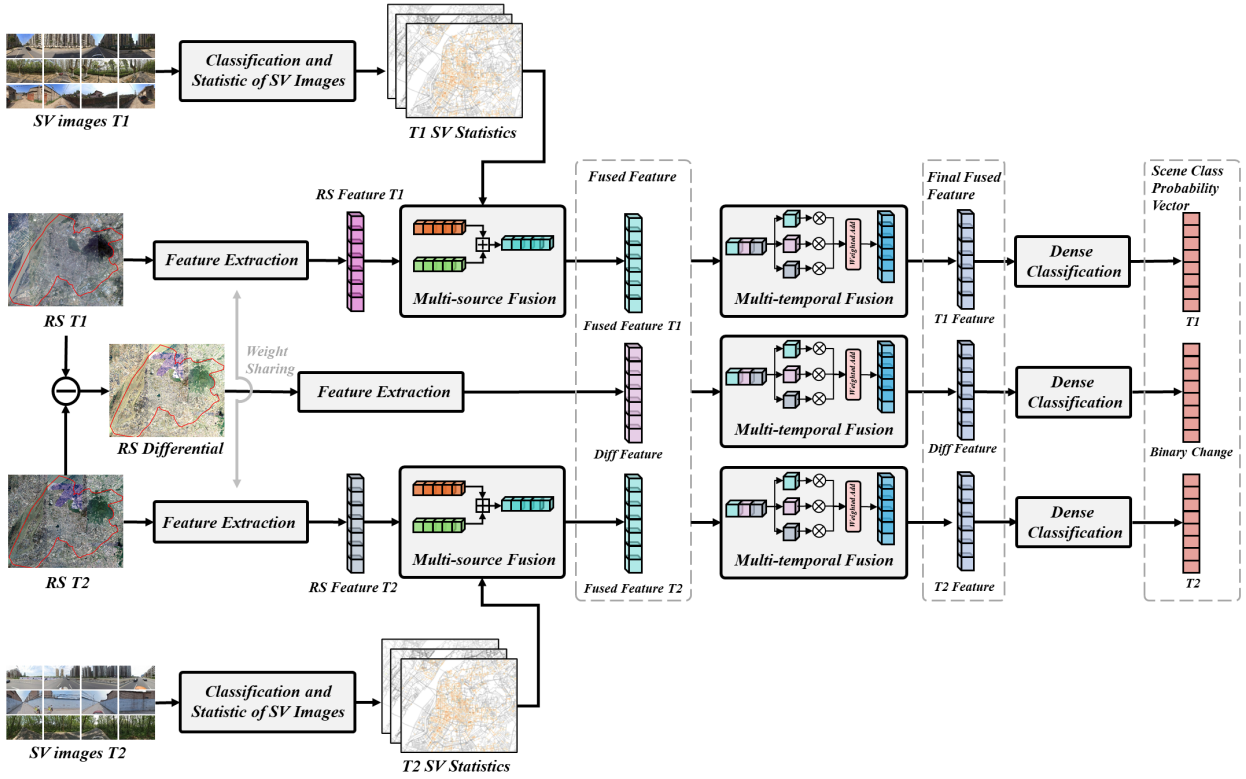


Overview of Chinese YSs research

Advancing Urban Monitoring: Urban Functional Zone Change Detection via Multi-Source Temporal Fusion of Street View and Remote Sensing Imagery

- The proposed method integrates multi-temporal **street view** and **remote sensing** imagery through **attention-based fusion** to achieve accurate UFZ change detection.

1. **SV Classification & Statistics:** Classify street view images at T1 and T2; compute category frequency maps for each UFZ.
2. **RS Feature Extraction:** Extract features from RS images at T1, T2, and their difference using CNNs.
3. **Multi-Source Feature Fusion:** Fuse SV and RS features with an attention-based fusion mechanism.
4. **Temporal Modeling:** Integrate temporal features using self-attention to capture changes over time.
5. **Final Classification:** Apply dense classification to fused features for UFZ change detection and labeling.

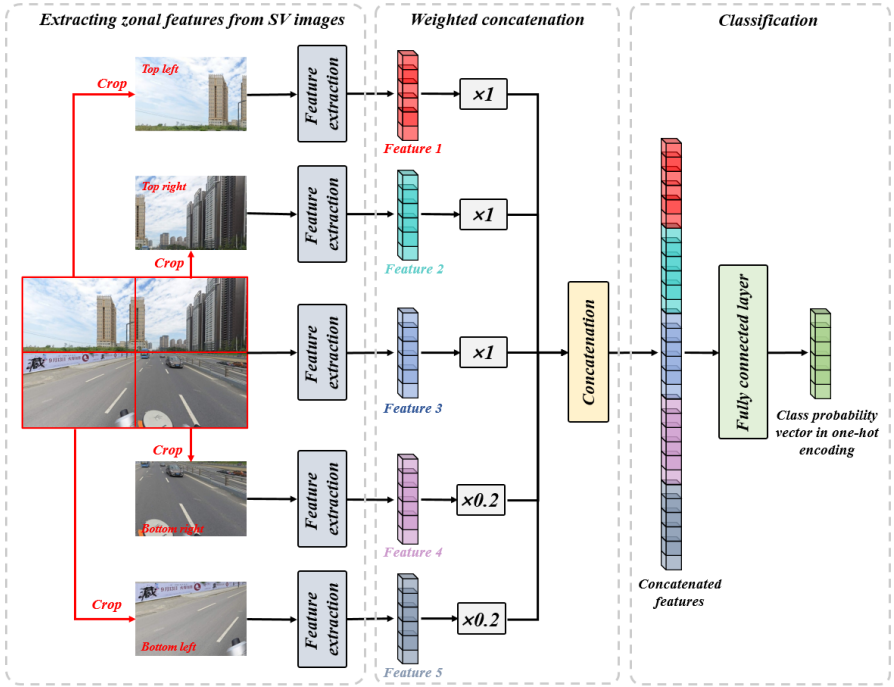


Overview of Chinese YSs research

Advancing Urban Monitoring: Urban Functional Zone Change Detection via Multi-Source Temporal Fusion of Street View and Remote Sensing Imagery

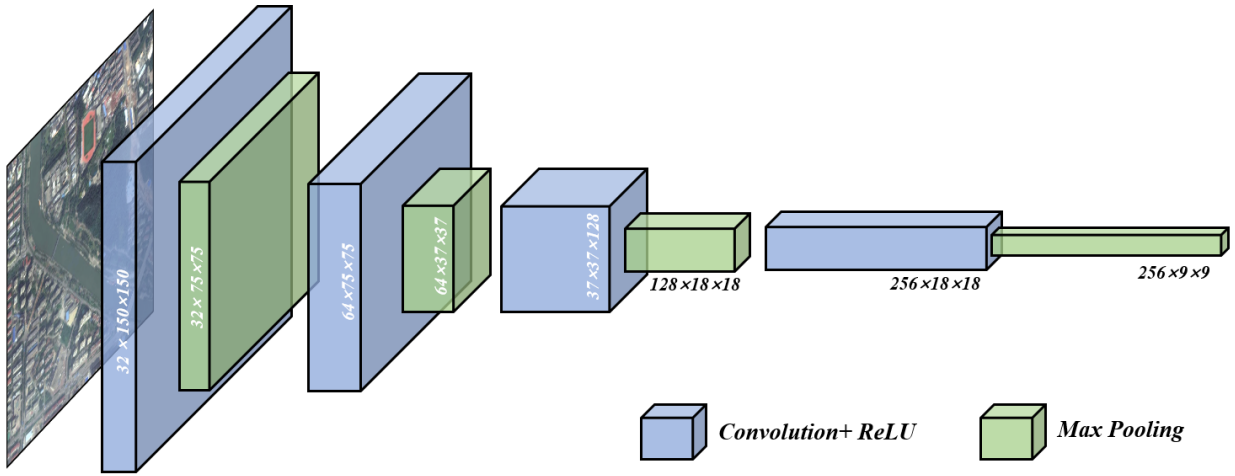
1. SV Classification & Statistics

SV images were classified into eight UFZ categories, and their spatial frequencies were aggregated into statistical raster maps aligned with RS data for fusion.



2. RS Feature Extraction

A multi-layer CNN extracts spatial features from RS imagery by progressively capturing both low- and high-level patterns, providing effective inputs for UFZ classification.



Overview of Chinese YSs research

Advancing Urban Monitoring: Urban Functional Zone Change Detection via Multi-Source Temporal Fusion of Street View and Remote Sensing Imagery

3. Multi-Source Feature Fusion

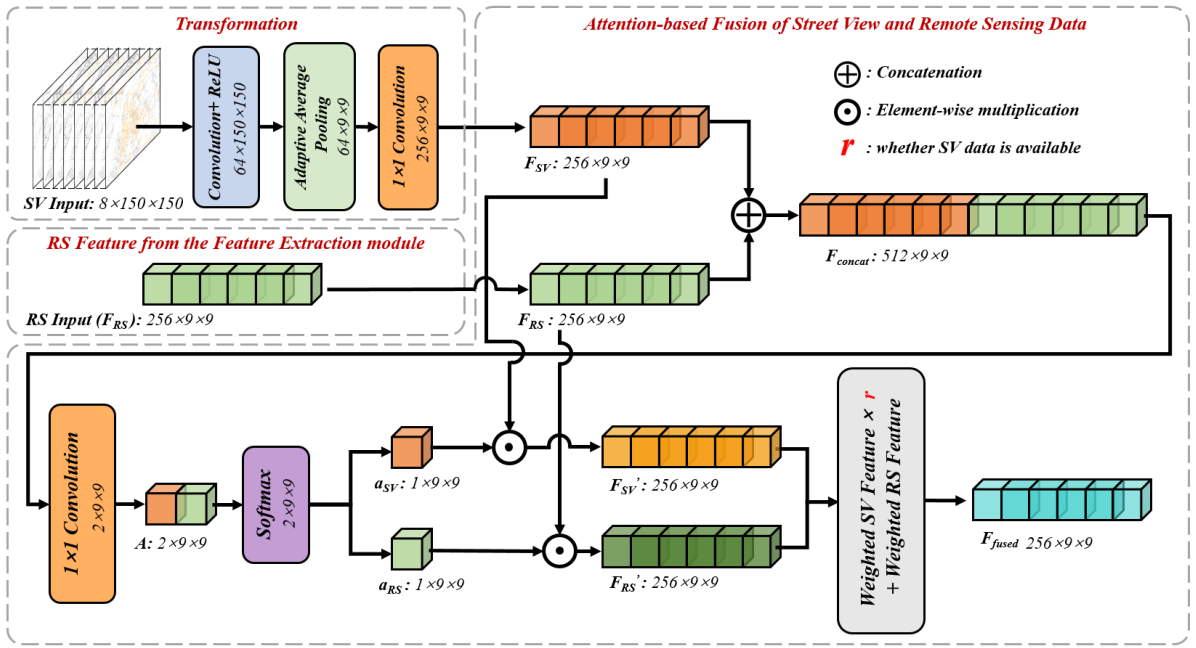
An attention-based fusion module aligns and integrates RS and SV features, adaptively weighting their contributions based on relevance and data availability to produce robust UFZ representations.

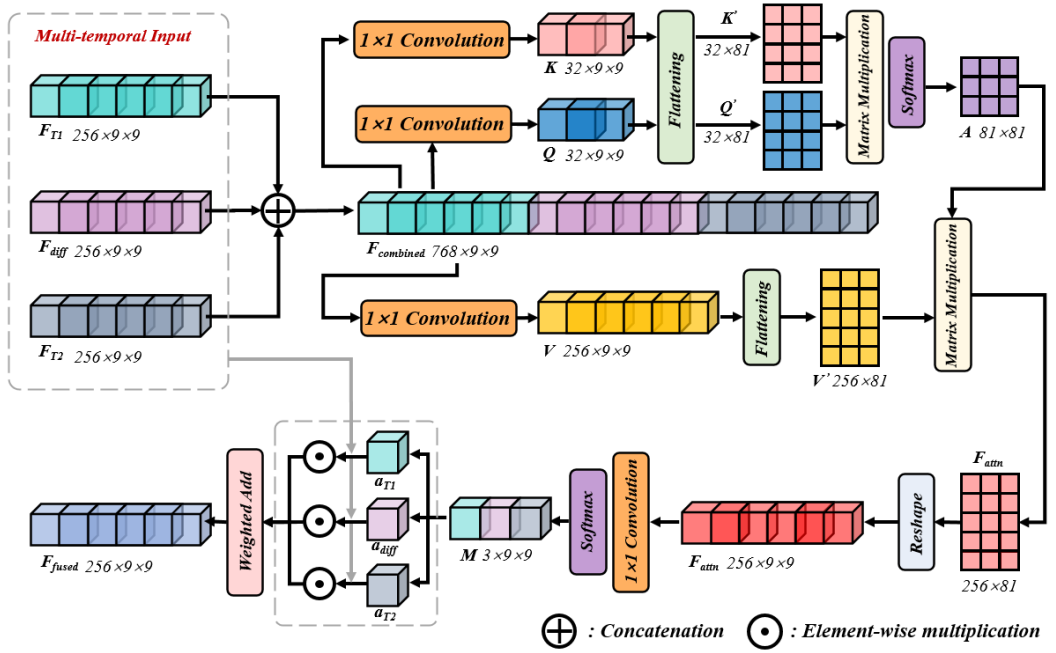
4. Temporal Modeling

A self-attention-based temporal fusion module integrates features from T1, T2, and their difference, dynamically weighting each time step to enhance change detection accuracy.

5. Final Classification

A fully connected classification module maps the fused features to target classes, producing the final UFZ change detection result.





Overview of Chinese YSs research

Advancing Urban Monitoring: Urban Functional Zone Change Detection via Multi-Source Temporal Fusion of Street View and Remote Sensing Imagery

- Five **baseline methods** (VGG16, ResNet18, DSIFN, FC-EF, DAN-CPFS) were **compared** under RS-only and RS+SV configurations, and tested across Nanjing, Chengdu, and Datong. All models were trained under the same settings. **Performance was evaluated** using Overall Accuracy and Kappa coefficient.

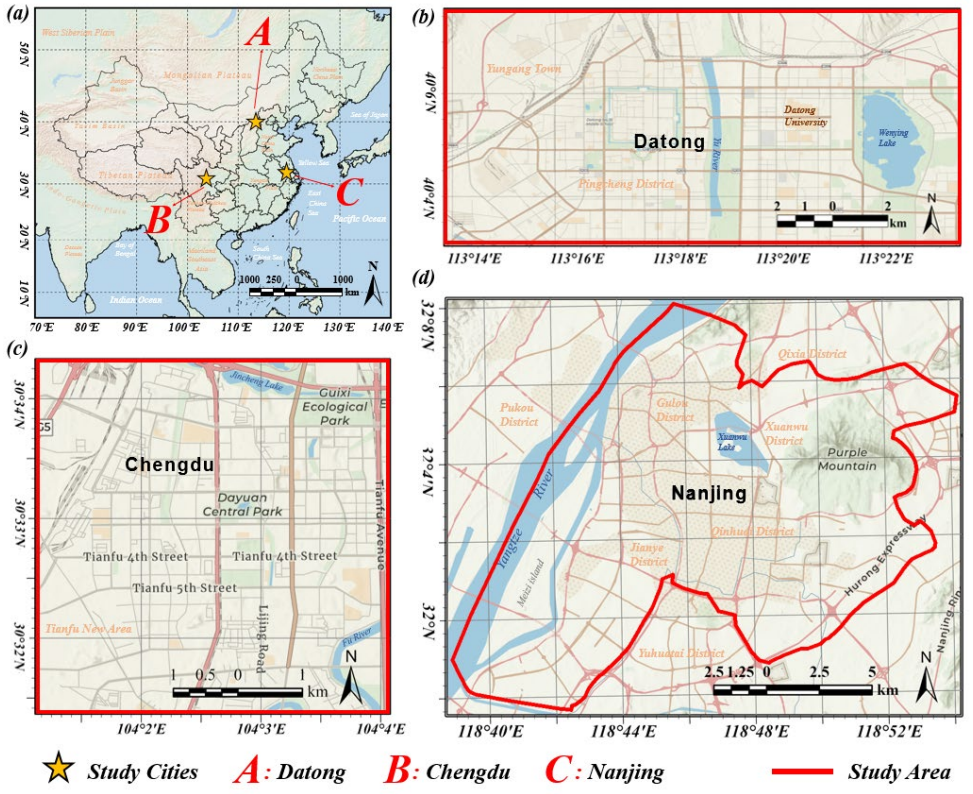


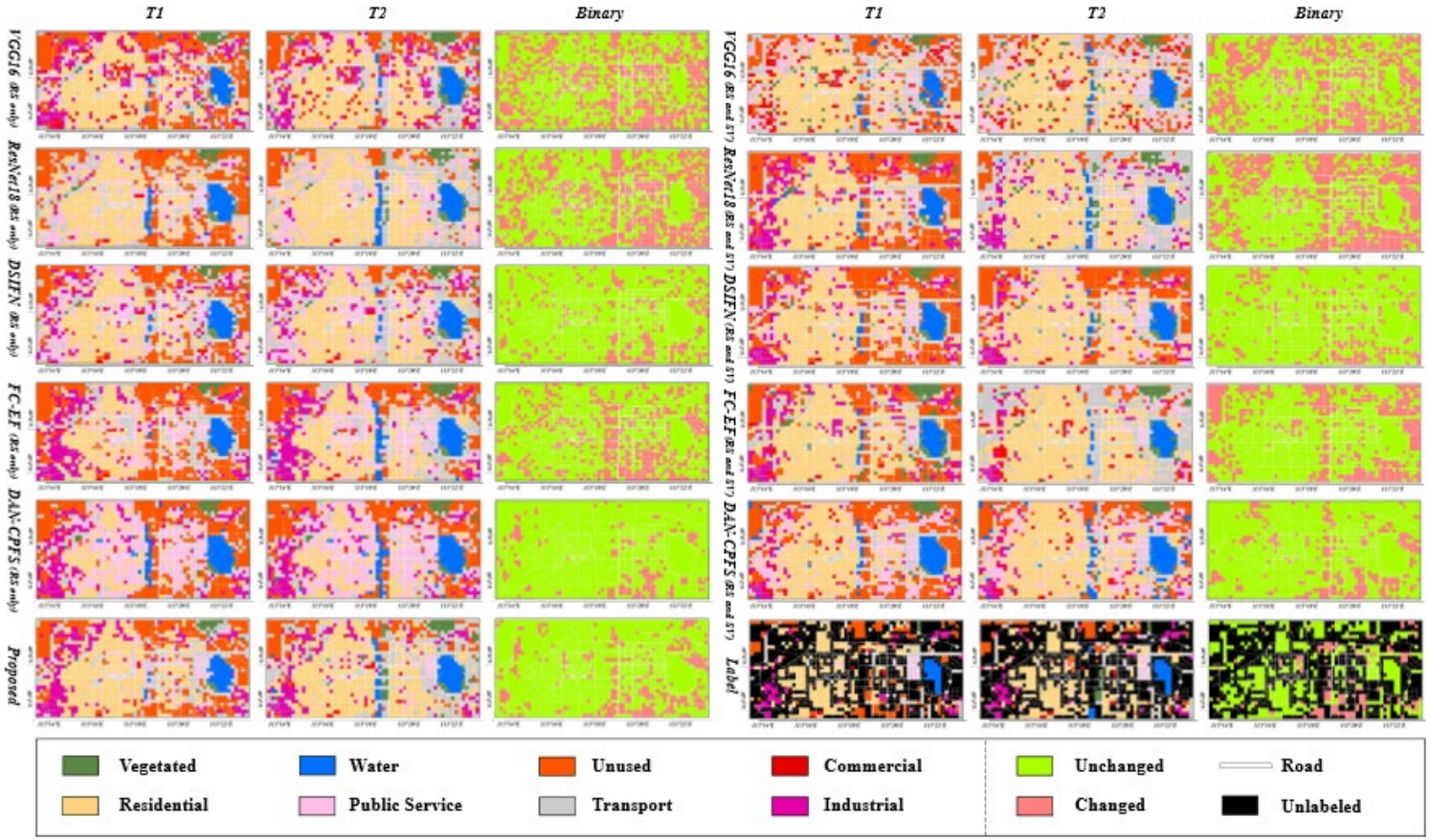
TABLE Accuracies of different methods over the Datong dataset

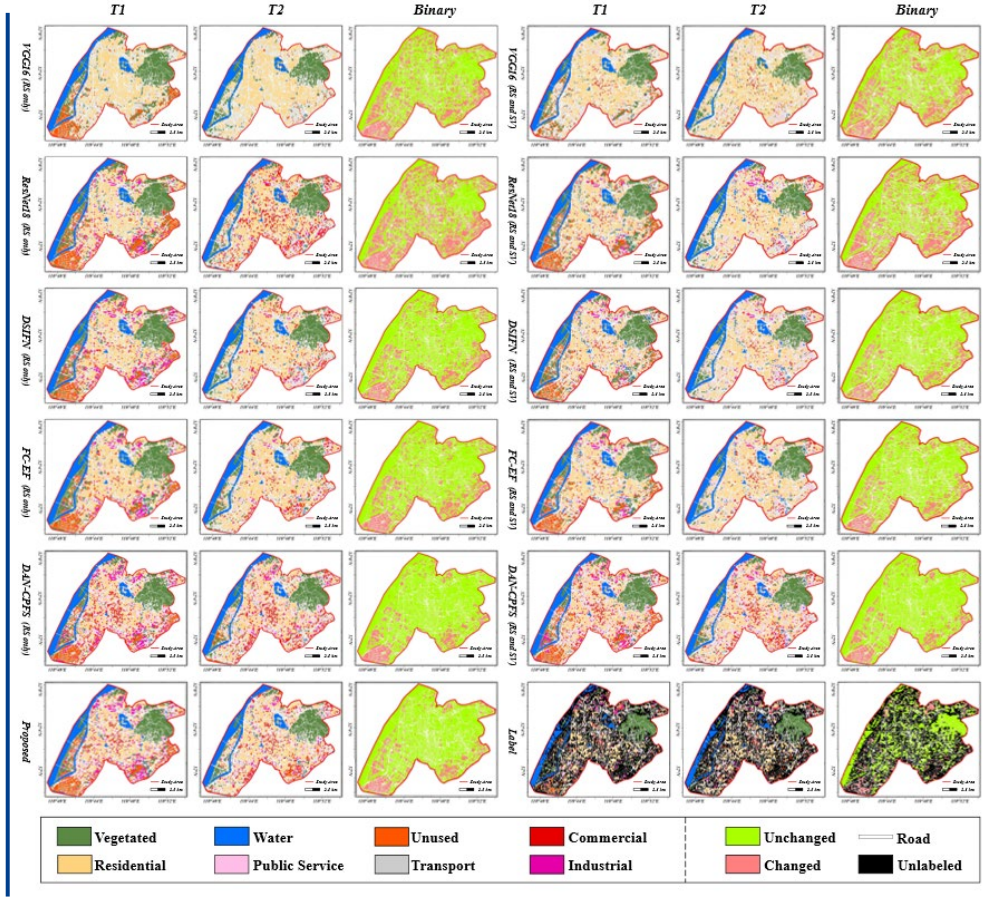
	Method	OA_1 (%)	OA_2 (%)	OA_B (%)	Kappa_1	Kappa_2	Kappa_B
RS only	VGG16	70.19	66.83	75.00	0.6114	0.5652	0.4007
	ResNet18	76.44	72.60	78.85	0.6819	0.6266	0.5000
	DSIFN	74.04	75.96	85.10	0.6606	0.6799	0.5061
	FC-EF	83.17	78..85	84.13	0.7741	0.7118	0.5296
	DAN-CPFS	84.13	74.04	87.98	0.7917	0.6574	0.5855
RS and SV	VGG16	72.60	67.79	77.40	0.6482	0.5762	0.4545
	ResNet18	85.10	75.00	77.40	0.8020	0.6702	0.4769
	DSIFN	83.17	79.33	79.81	0..7761	0.7194	0.3374
	FC-EF	78.37	66.83	73.08	0.7144	0.5493	0.3158
	DAN-CPFS	82.69	78.85	90.38	0.7714	0.7128	0.6782
	Proposed	**85.58**	**85.58**	**90.87**	**0.8058**	**0.8059**	**0.6973**

Overview of Chinese YSs research

Advancing Urban Monitoring: Urban Functional Zone Change Detection via Multi-Source Temporal Fusion of Street View and Remote Sensing Imagery

- The proposed method **outperformed** baseline models in three reseach areas, showing **higher spatial consistency** and boundary precision, and accurately capturing urban transitions.



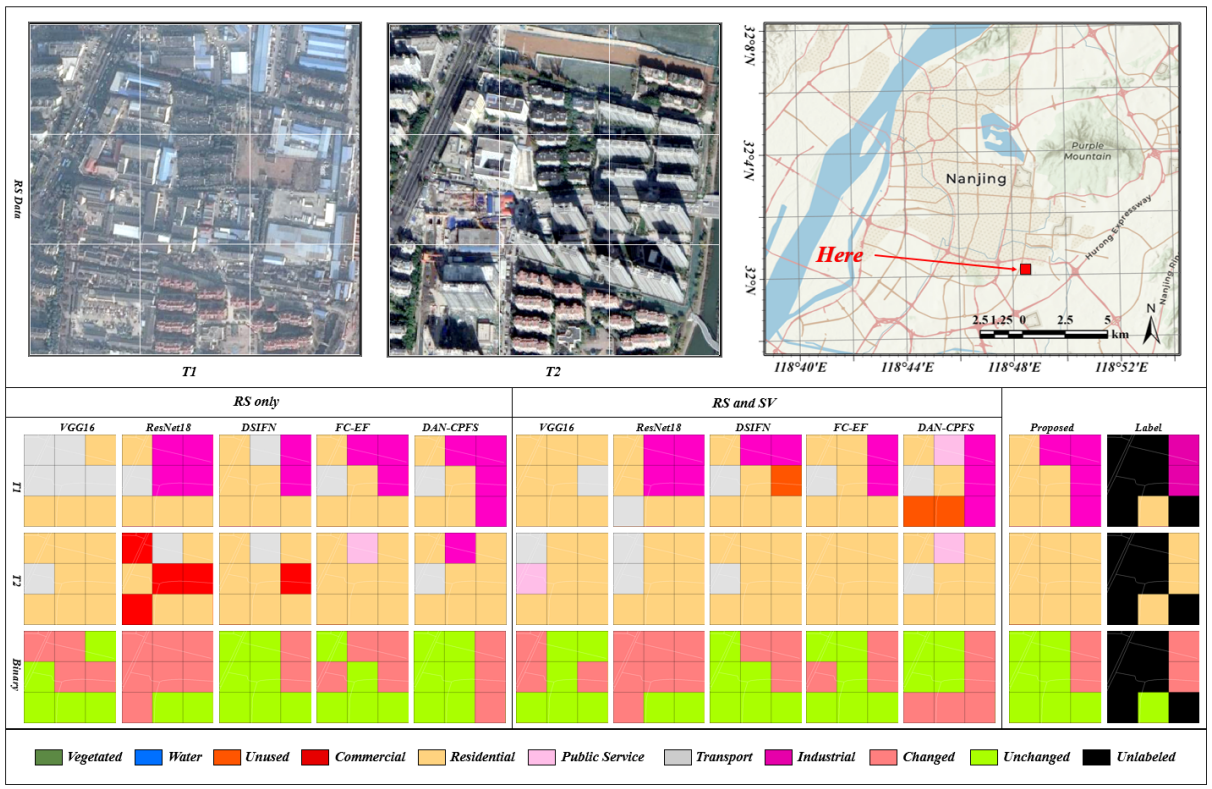


Overview of Chinese YSs research

Advancing Urban Monitoring: Urban Functional Zone Change Detection via Multi-Source Temporal Fusion of Street View and Remote Sensing Imagery

- Two **representative areas**—Hexi and Daming Road—were analyzed to illustrate UFZ transitions. The proposed method **accurately detected functional changes** from industrial and unused zones to residential and public service, outperforming RS-only models by leveraging SV data for improved temporal consistency and spatial precision.

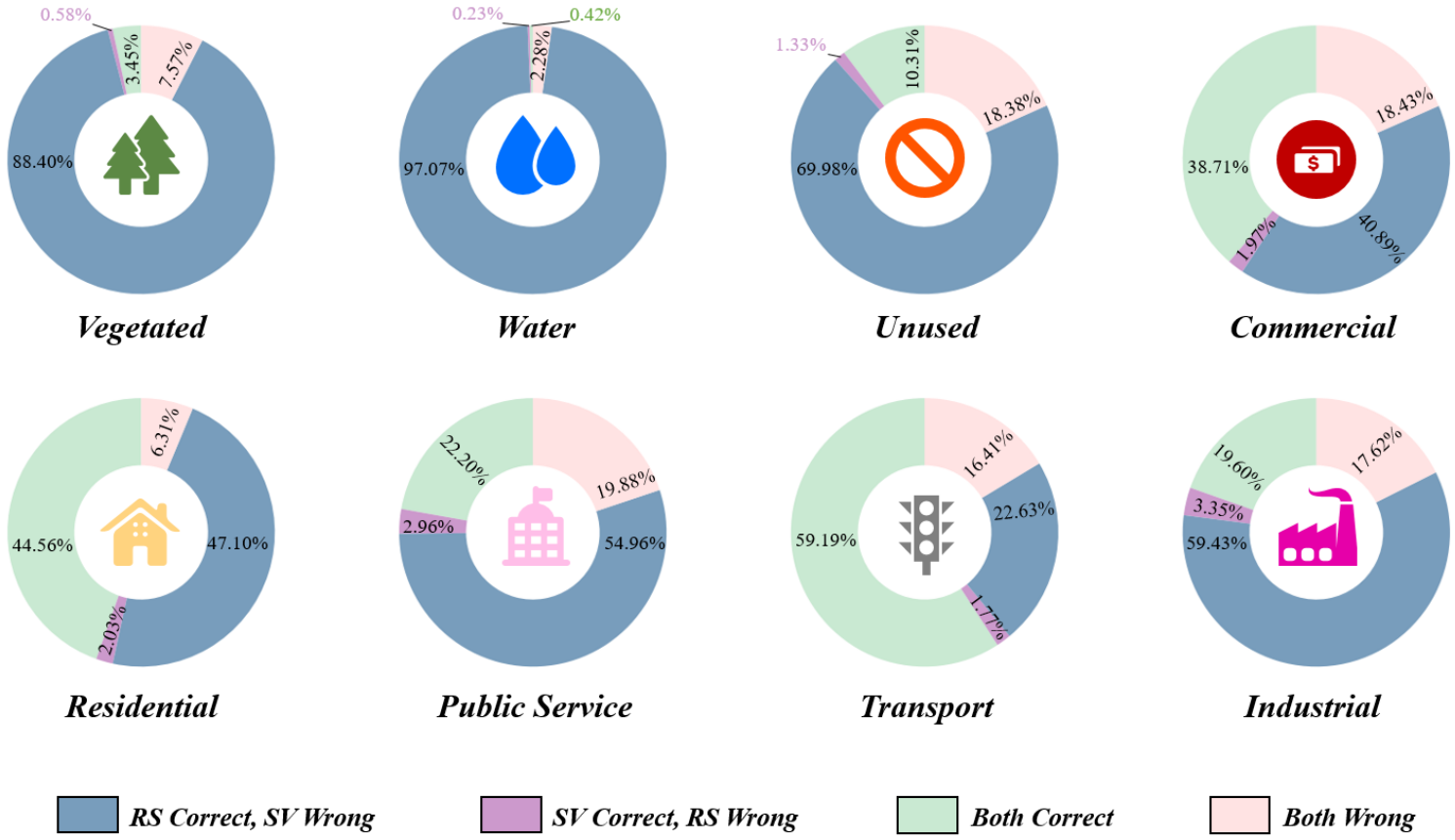




Overview of Chinese YSs research

Advancing Urban Monitoring: Urban Functional Zone Change Detection via Multi-Source Temporal Fusion of Street View and Remote Sensing Imagery

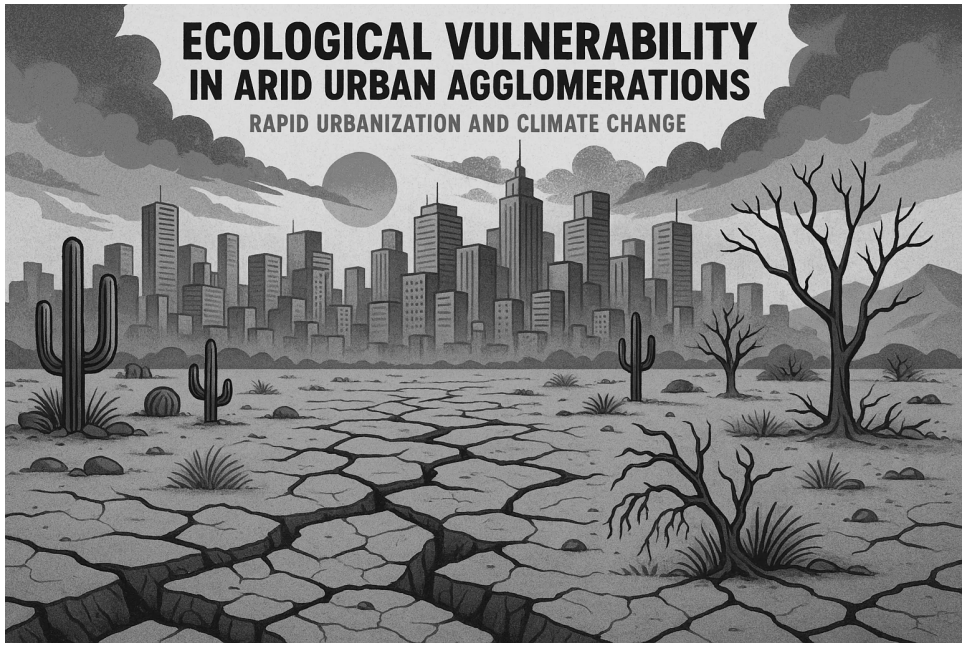
- RS data performed well in **large, homogeneous zones** like Vegetated and Water, while SV data provided valuable ground-level details in **complex areas** such as Commercial and Transport.
- For zones like Residential and Public Service, both data **types contributed complementary information**.
- This highlights the **importance of integrating** RS and SV for accurate UFZ classification.



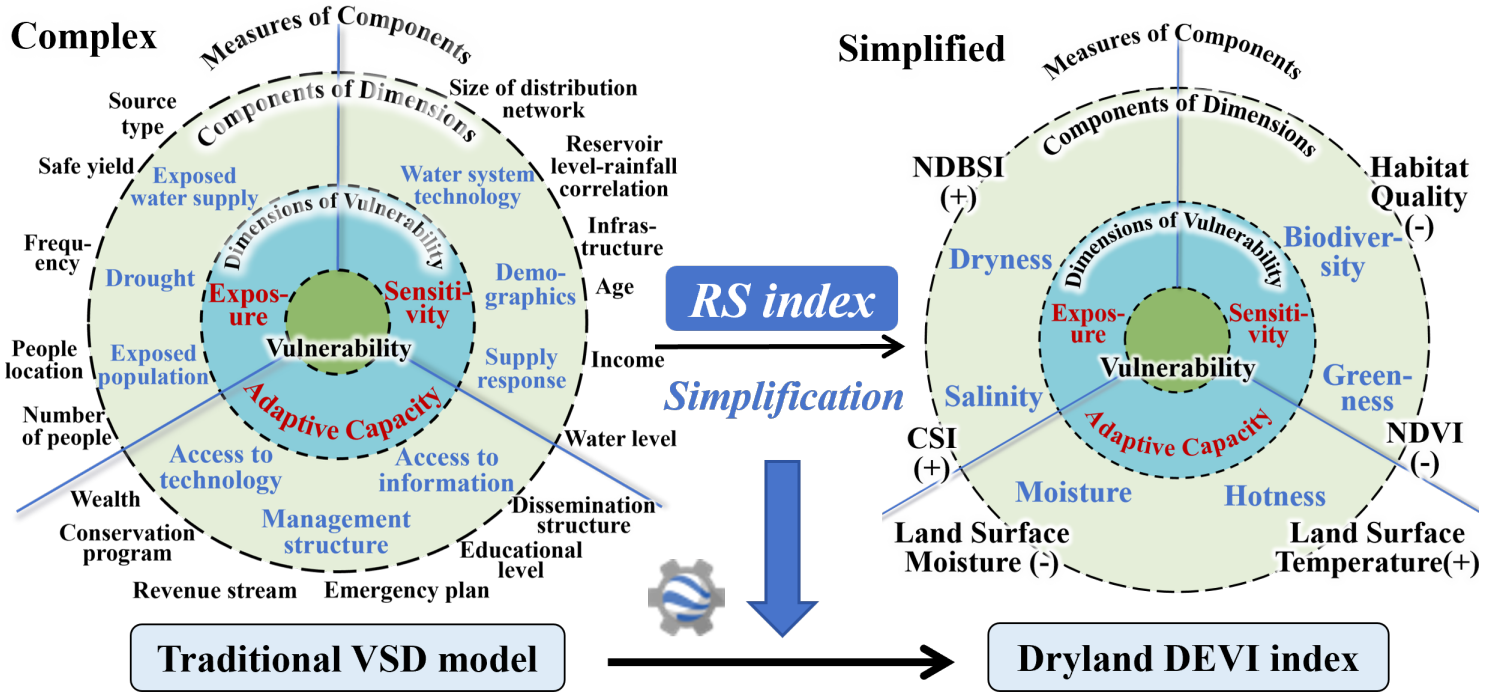
Overview of Chinese YSs research

Advancing Urban and Environmental Resilience : Dynamic monitoring of fine-grained ecological vulnerability in dryland urban agglomeration integrating novel remote sensing index and explainable machine learning

- Rapid urbanization and climate change threaten the ecological vulnerability in arid urban agglomerations, posing risks to sustainability and ecosystem stability.
- Here, a novel dryland ecological vulnerability index (DEVI) is proposed to simplify the traditional complex vulnerability scoping diagram (VSD) and monitor ecological changes in arid city clusters from 1986-2024.

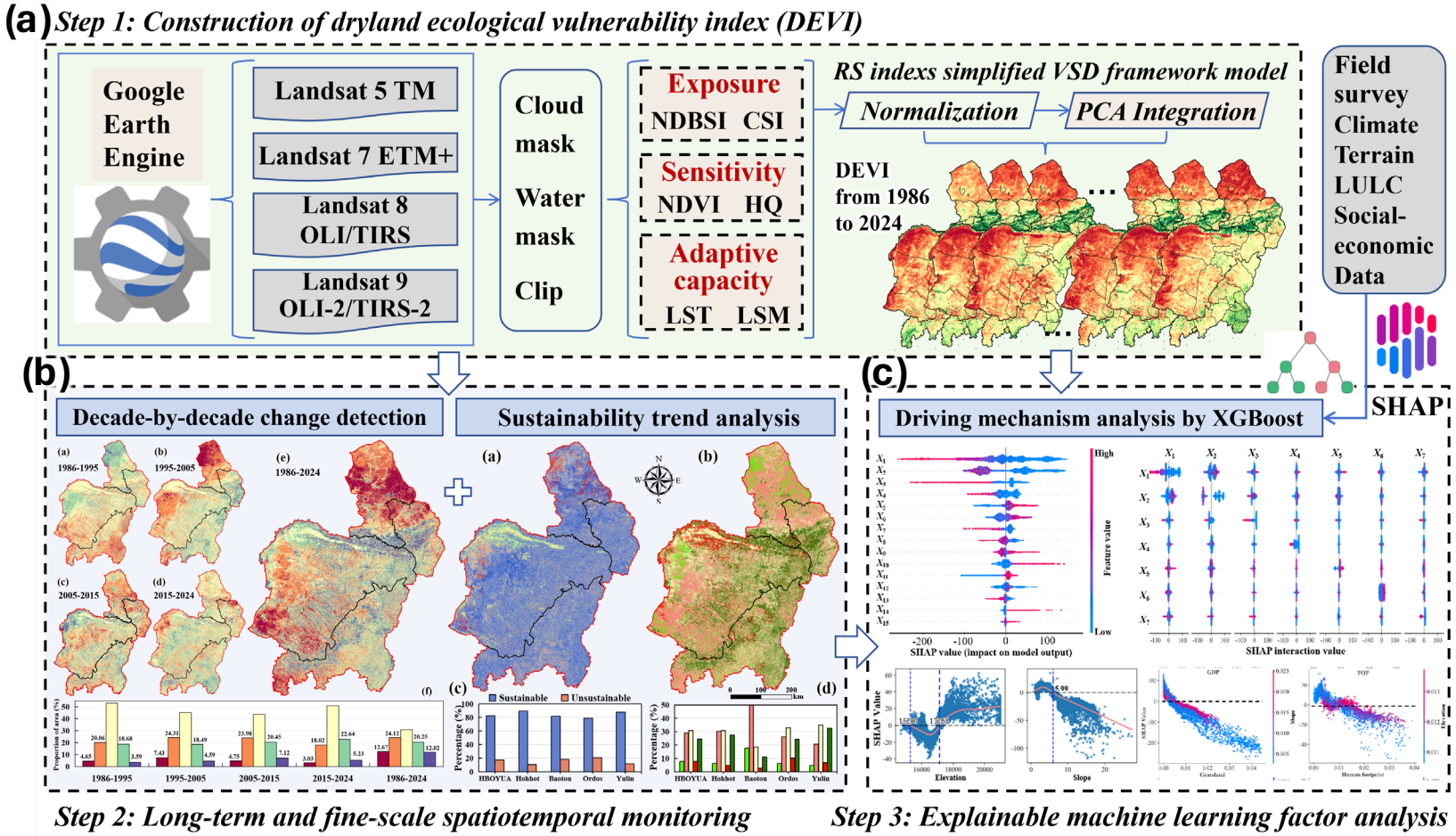


Dryland urbanization affects ecological vulnerability



Overview of Chinese YSs research

Advancing Urban and Environmental Resilience : Dynamic monitoring of fine-grained ecological vulnerability in dryland urban agglomeration integrating novel remote sensing index and explainable machine learning



A long-term fine-grained vulnerability monitoring framework for dryland urban agglomerations:

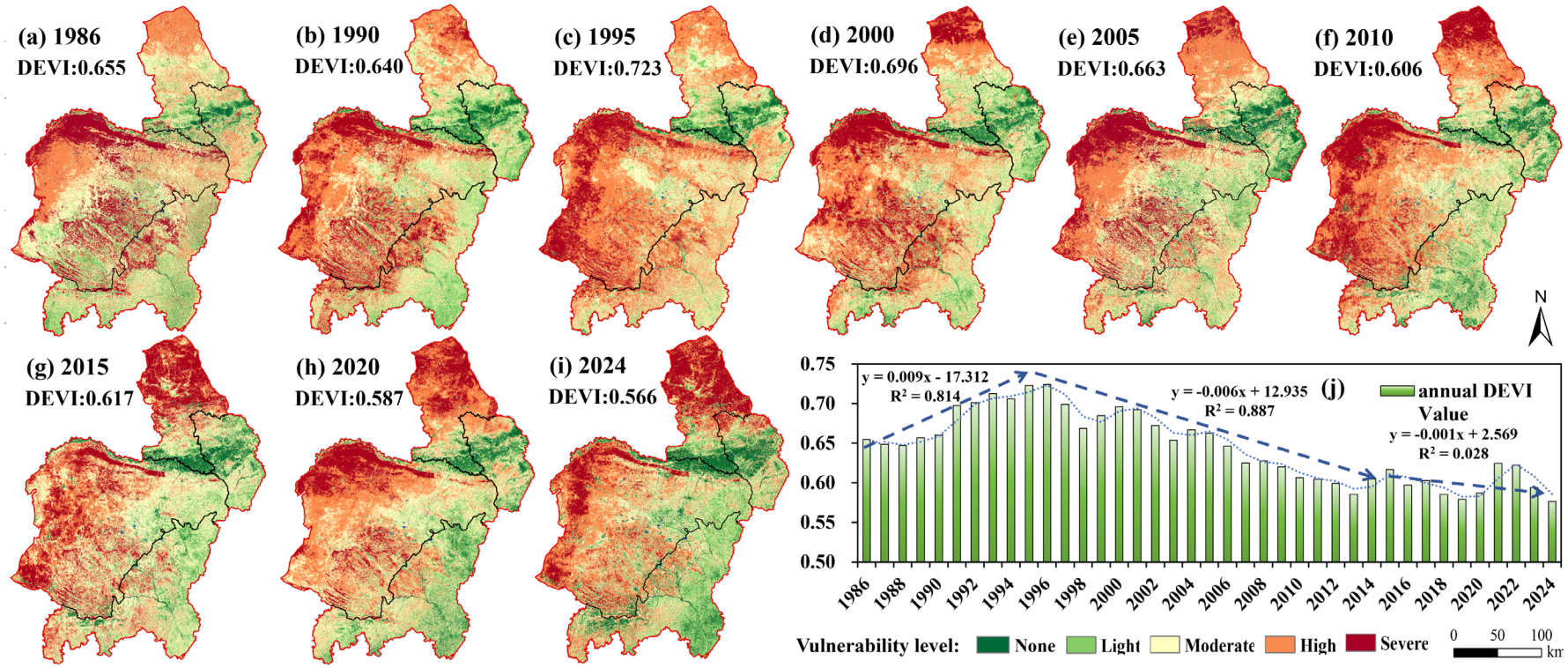
- **Six key ecological indicators** derived through remote sensing simplified the traditional VSD framework **to construct DEVI**. (a).
- Spatiotemporal patterns were then analyzed to identify historical trends and predict future sustainability. (b).
- XGBoost was coupled with SHAP method to **model** and **visualize the impact of vulnerability factors**.(c).

Chunqiang Li, Shanchuan Guo, Qin Huang, Haowei Mu, Bo Yuan, Zilong Xia, … , **Peijun Du***. (2025). Dynamic monitoring of fine-grained ecological vulnerability in dryland urban agglomeration integrating novel remote sensing index and explainable machine learning. ***GIScience & Remote Sensing***, 62(1).

Overview of Chinese YSs research

Advancing Urban and Environmental Resilience : Dynamic monitoring of fine-grained ecological vulnerability in dryland urban agglomeration integrating novel remote sensing index and explainable machine learning

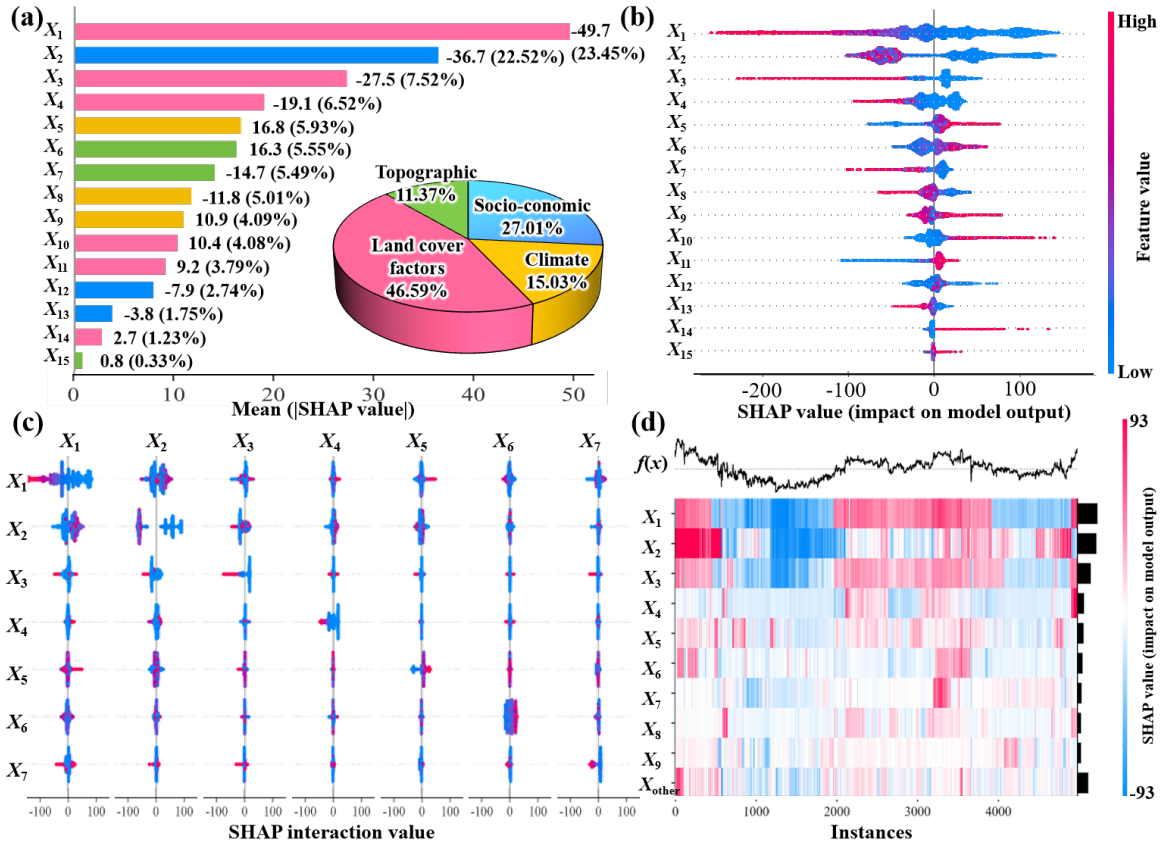
- **Temporally,** over nearly 40 years, DEVI initially increased, then decreased, indicating ecological conditions first deteriorated and then improved, with an overall improvement of 14%.
- **Spatially,** vulnerability reduced in Loess Hills but remained high in Ordos Plateau and northern Inner Mongolia, with degradation areas still exceeding improvements by 4.5%, reflecting **an imbalance in current ecological governance**.

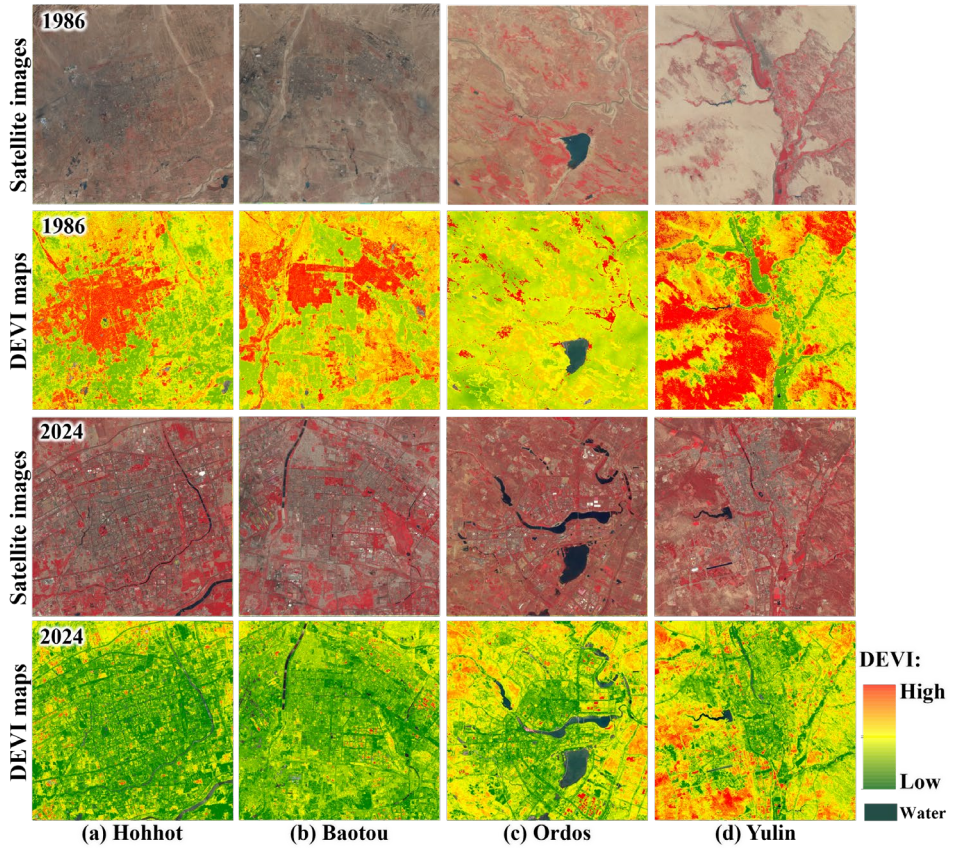


Overview of Chinese YSs research

Advancing Urban and Environmental Resilience : Dynamic monitoring of fine-grained ecological vulnerability in dryland urban agglomeration integrating novel remote sensing index and explainable machine learning

- Improved areas have been increasing, mainly driven by land restoration (46.6%) and socioeconomic factors (27.0%), **SHAP analysis** also identified the thresholds and interaction effects of key drivers. (Left)
- Urban expansion in the arid city cluster improved surrounding ecosystems and decreased ecological vulnerability.

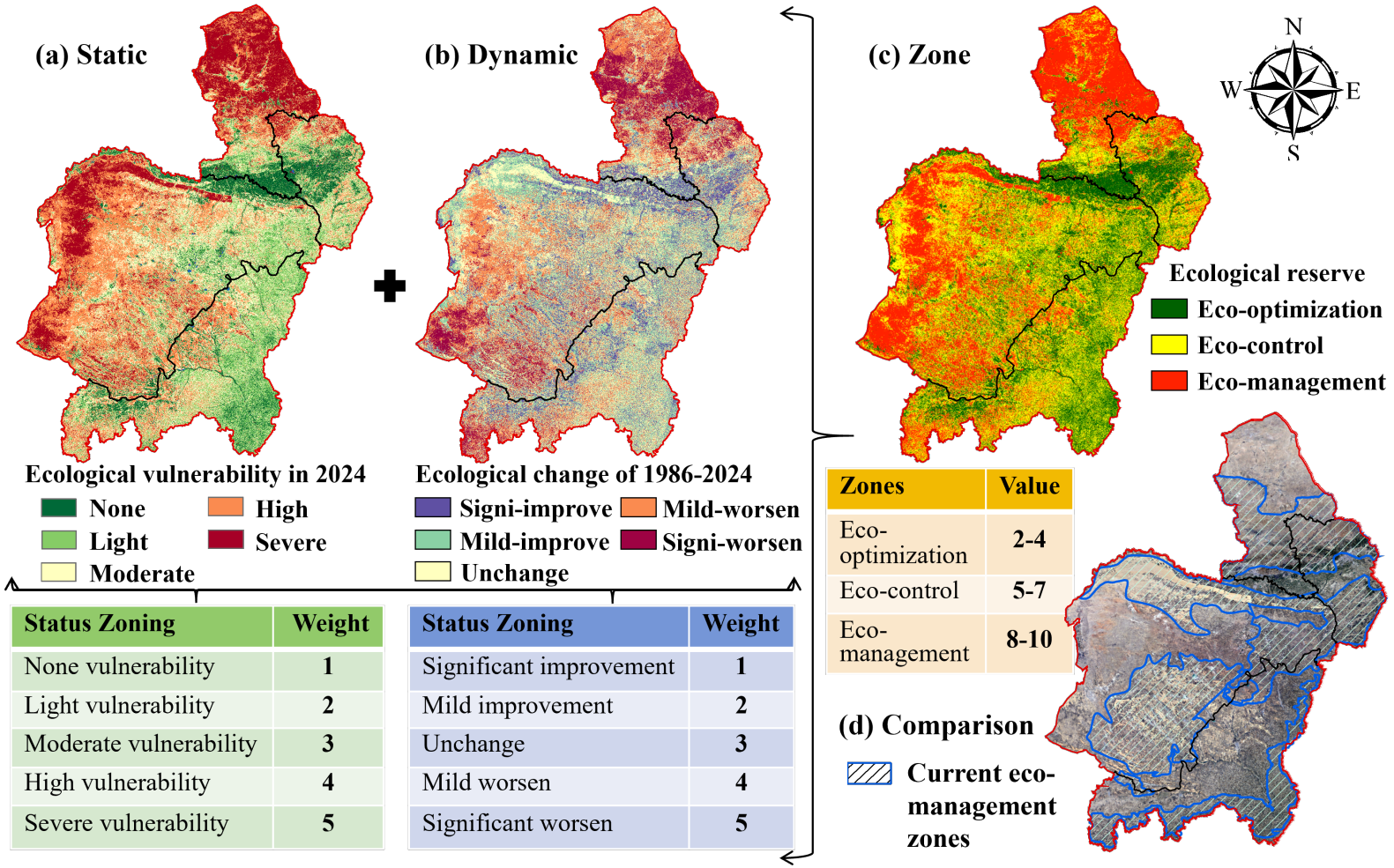




Chunqiang Li, Shanchuan Guo, … , **Peijun Du***. (2025). Dynamic monitoring of fine-grained ecological vulnerability in dryland urban agglomeration integrating novel remote sensing index and explainable machine learning.

Overview of Chinese YSs research

Advancing Urban and Environmental Resilience : Dynamic monitoring of fine-grained ecological vulnerability in dryland urban agglomeration integrating novel remote sensing index and explainable machine learning



Status Zoning	Weight
None vulnerability	1
Light vulnerability	2
Moderate vulnerability	3
High vulnerability	4
Severe vulnerability	5

Status Zoning	Weight
Significant improvement	1
Mild improvement	2
Unchange	3
Mild worsen	4
Significant worsen	5

Zones	Value
Eco-optimization	2-4
Eco-control	5-7
Eco-management	8-10

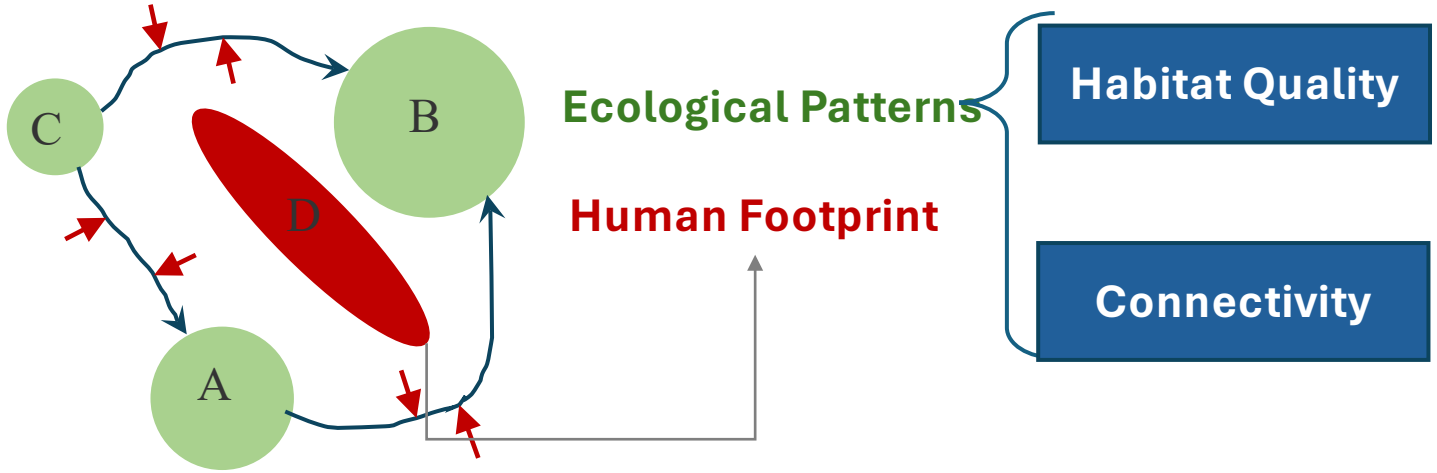
- Integrate static vulnerability conditions and dynamic changes to propose new ecological management areas and compare planning scenarios.
- **Discrepancies exist in current ecological management zones**, especially in the **southwestern Ordos Plateau and northern Inner Mongolia Plateau**, where **severe vulnerability remains unmanaged**.
- Future ecological management should **integrate static and dynamic conditions**, **adjusting timely** to enhance sustainability decisions.

Chunqiang Li, Shanchuan Guo, Qin Huang, Haowei Mu, Bo Yuan, Zilong Xia, … , **Peijun Du***. (2025). Dynamic monitoring of fine-grained ecological vulnerability in dryland urban agglomeration integrating novel remote sensing index and explainable machine learning. ***GIScience & Remote Sensing***, 62(1).

Overview of Chinese YSs research

Environmental Resilience: Quantifying the anthropogenic sensitivity of ecological patterns in arid urban agglomeration



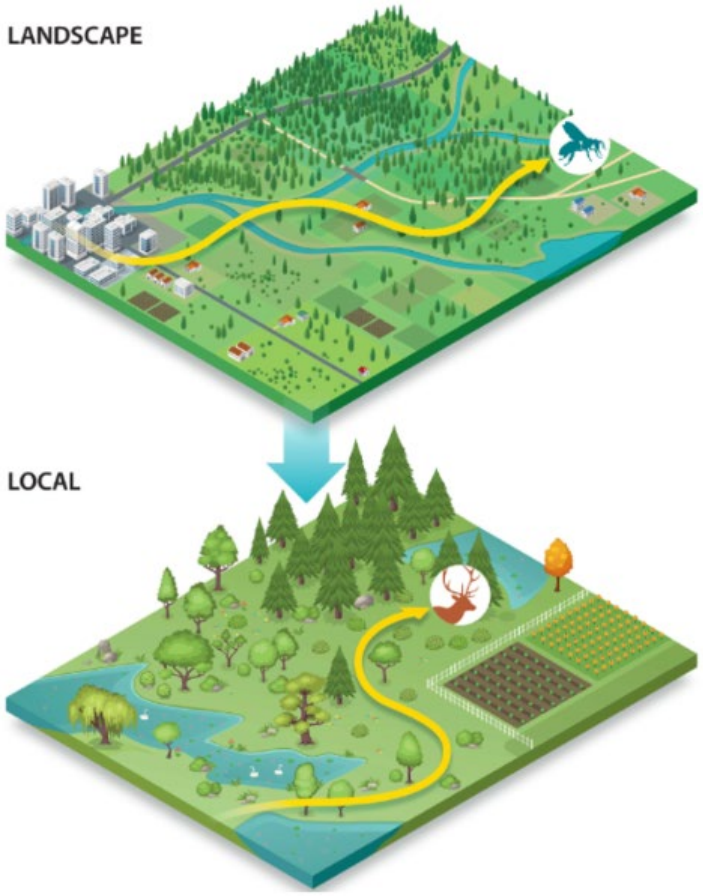


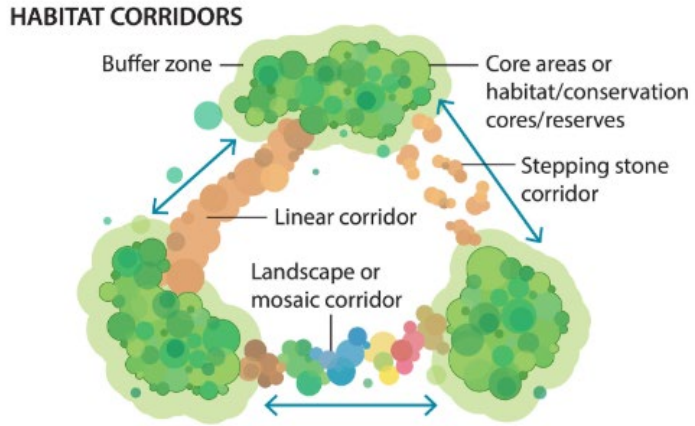


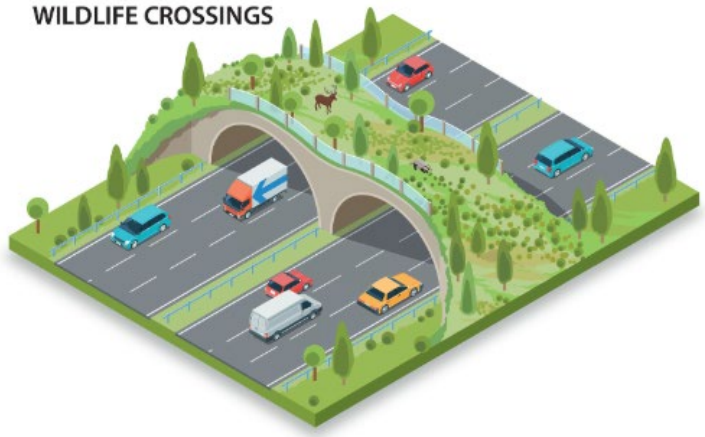
Hilty, J., Worboys, G. L., Keeley, A., Woodley, S., Lausche, B. J., Locke, H., ... & Tabor, G. M. (2020). Guidelines for conserving connectivity through ecological networks and corridors. **International Union for Conservation of Nature, Global Protected Areas Programme**

Overview of Chinese YSs research

Environmental Resilience: A well-connected Earth, environmental contributions of connectivity research





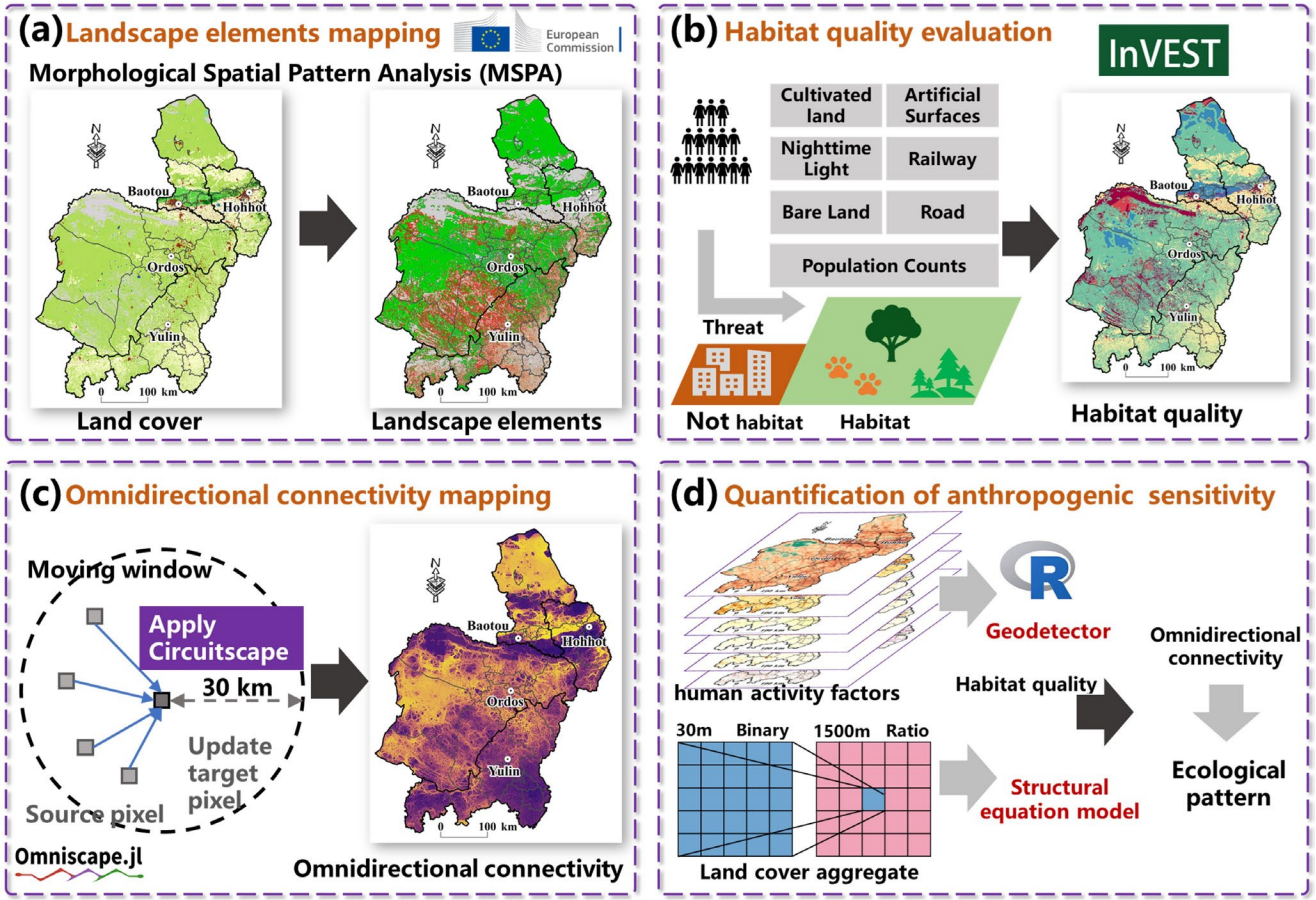


- **Enhancing Ecological Functions:** Connectivity improving ecological functions and services while reducing extinction risks.
- **Supporting Ecological Processes and Services:** Connectivity facilitates species movement, maintaining population dynamics and vital ecosystem services like strengthening environmental resilience.
- **Climate Adaptation and Ecosystem Restoration:** Connectivity enables species to migrate in response to climate change and provides a foundation for restoring ecological corridors, aiding environmental adaptation.

Brodie, Jedediah F., et al. A well-connected Earth: The science and conservation of organismal movement[J]. ***Science***, 2025, 388.6745 : eadn2225.
Brennan, A., et al. Functional connectivity of the world's protected areas[J]. ***Science***, 2022, 376.6597: 1101-1104.

Overview of Chinese YSs research

Environmental Resilience: **Quantifying the anthropogenic sensitivity of ecological patterns in arid urban agglomeration**



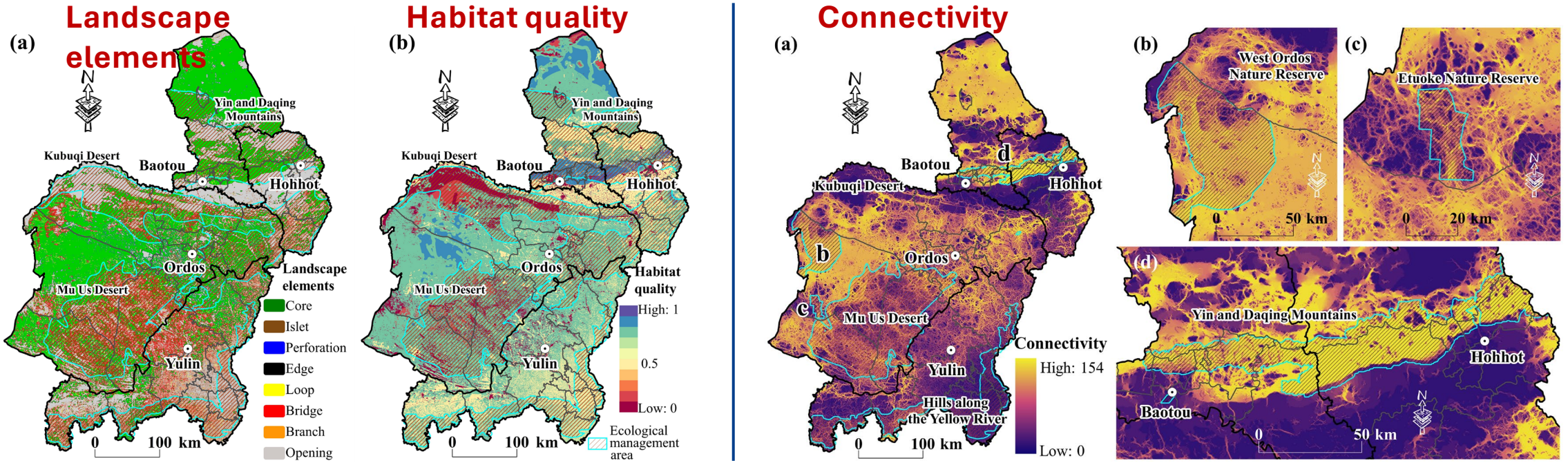
- Morphological Spatial Pattern Analysis (MSPA) was applied to identify and classify landscape elements, **providing a foundation for understanding regional ecological structures** (a).
- Habitat quality (InVEST) and connectivity (Circuit model) were evaluated. **This integration offered detailed insights into regional ecological** (b, c).
- Geodetector and structural equation modeling (SEM) were used to explore the **causal mechanisms** and quantify the **path coefficients** of anthropogenic sensitivity (d).

Haowei Mu, Shanchuan Guo, Xingang Zhang, Bo Yuan, Chunqiang Li, **Peijun Du***. (2025). Quantifying the anthropogenic sensitivity of ecological patterns in arid urban agglomeration. ***Applied Geography***, 178, 103595.

Overview of Chinese YSs research

Environmental Resilience: Quantifying the anthropogenic sensitivity of ecological patterns in arid urban agglomeration

- Landscape elements and habitat quality exhibit clear spatial correlations (Left).
- In the Kubuqi Desert, **patch-like corridors** help prevent wind and stabilize sand, while the **strip-like corridors** in the Mu Us Desert aid ecological resource flow and support restoration. However, the latter are more vulnerable to human activities (Right).

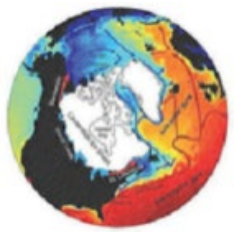


Haowei Mu, Shanchuan Guo, Xingang Zhang, Bo Yuan, Chunqiang Li, **Peijun Du***. (2025). Quantifying the anthropogenic sensitivity of ecological patterns in arid urban agglomeration. ***Applied Geography***, 178, 103595.

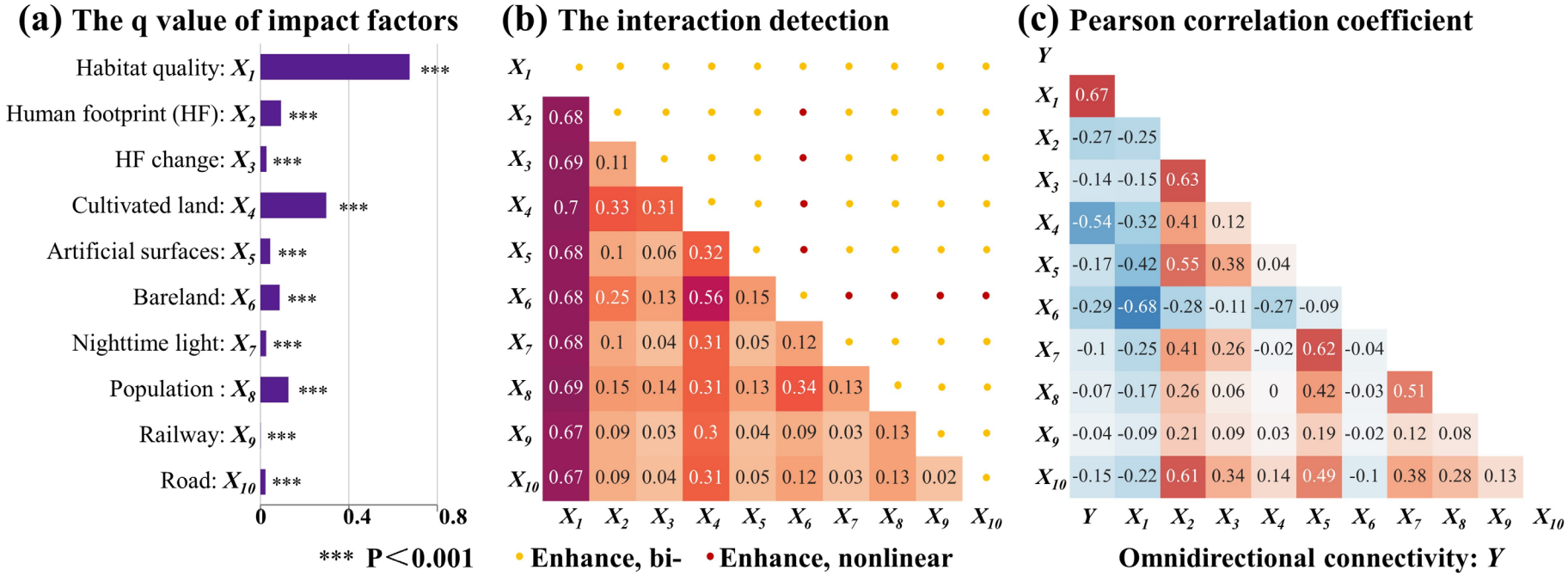
Overview of Chinese YSs research

Environmental Resilience: Quantifying the anthropogenic sensitivity of ecological patterns in arid urban agglomeration

- **Habitat Quality's Key Role:** Habitat quality (X1) is the most critical factor affecting connectivity, enhancing it and amplifying the influence of other factors like **cultivated land, population, and impervious surfaces**.
- **Human Activity Interactions:** The interaction between cultivated and bare land, significantly reduce habitat quality, increasing explanatory power by 88% and **negatively impacting connectivity**.



Geodetector



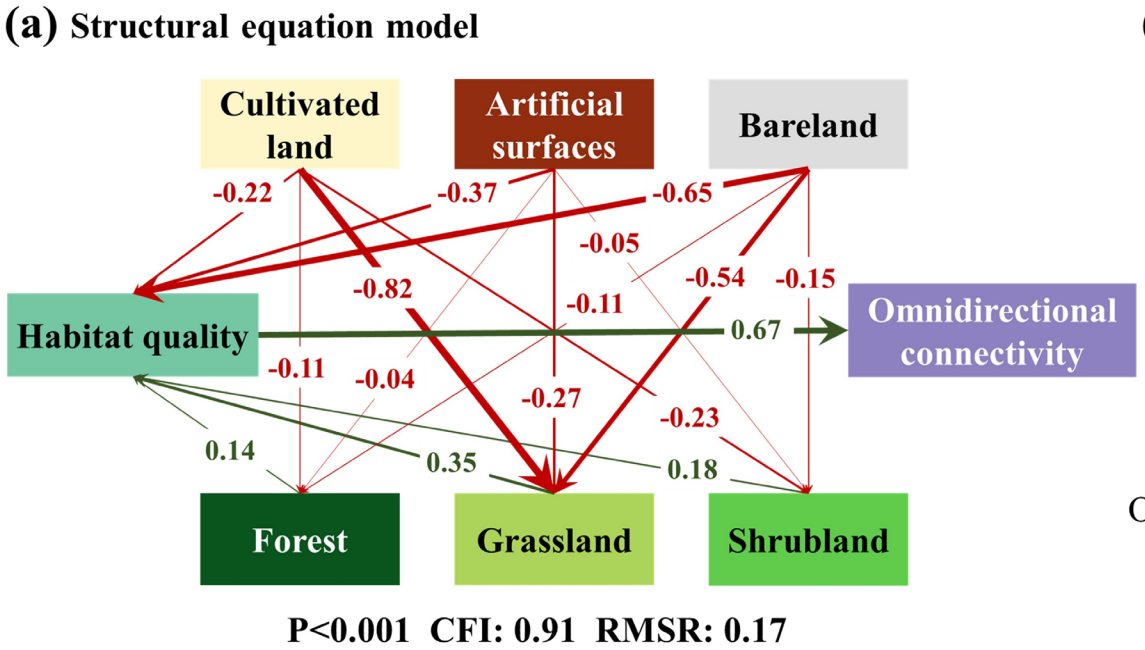
Haowei Mu, Shanchuan Guo, Xingang Zhang, Bo Yuan, Chunqiang Li, **Peijun Du***. (2025). Quantifying the anthropogenic sensitivity of ecological patterns in arid urban agglomeration. ***Applied Geography***, 178, 103595.

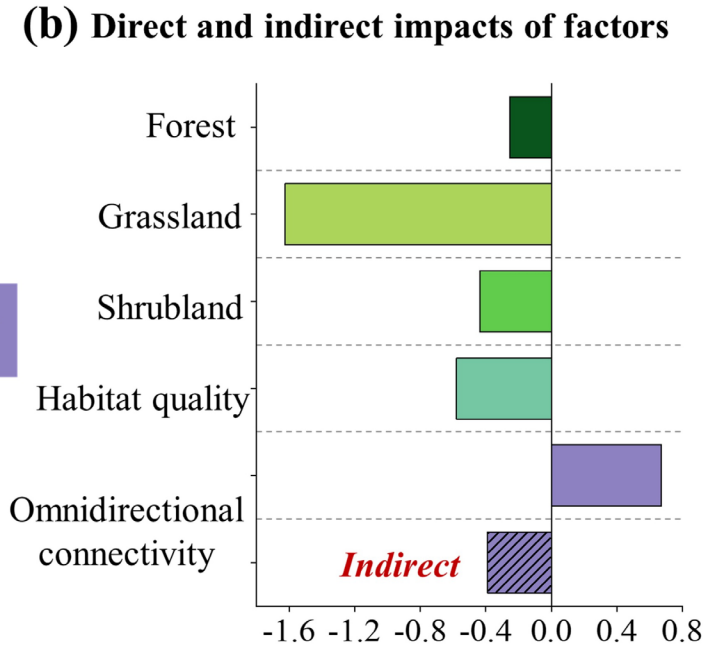
Overview of Chinese YSs research

Environmental Resilience: Quantifying the anthropogenic sensitivity of ecological patterns in arid urban agglomeration

- **Indirect Impacts:** Human activities, particularly cultivated land and impervious surfaces, **indirectly affect connectivity** by altering habitat quality, leading to negative impacts..
- **Path Analysis:** Habitat quality directly enhances connectivity (**path coefficient 0.67**), but other factors impose a total negative indirect impact on connectivity (**path coefficient −0.39**).

Structural equation model





Haowei Mu, Shanchuan Guo, Xingang Zhang, Bo Yuan, Chunqiang Li, **Peijun Du***. (2025). Quantifying the anthropogenic sensitivity of ecological patterns in arid urban agglomeration. ***Applied Geography***, 178, 103595.

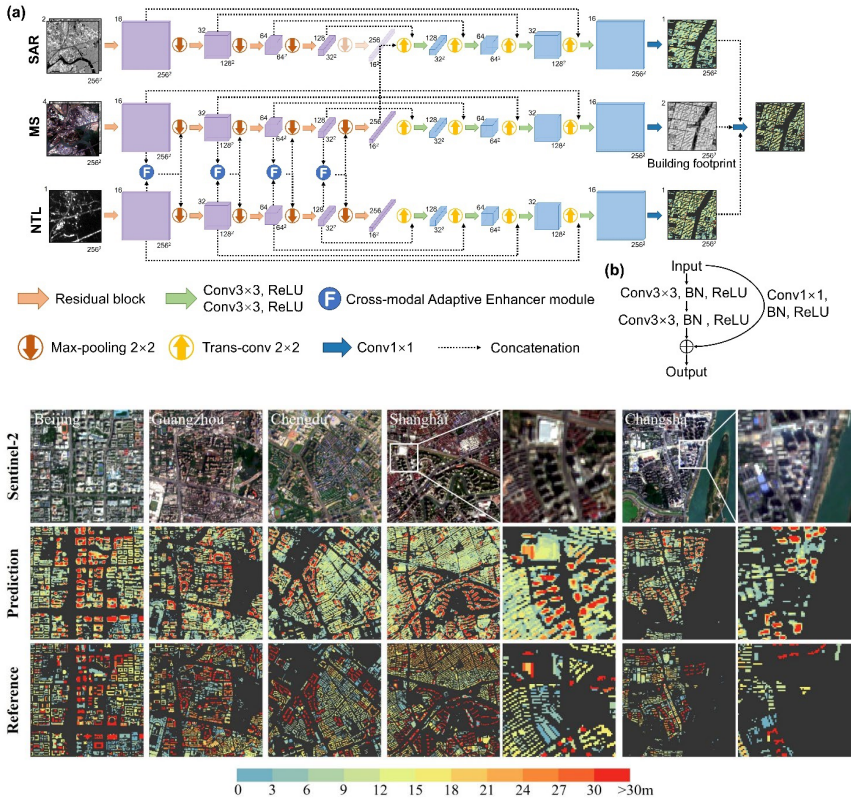
Chinese Young Scientists contributions in Dragon 6

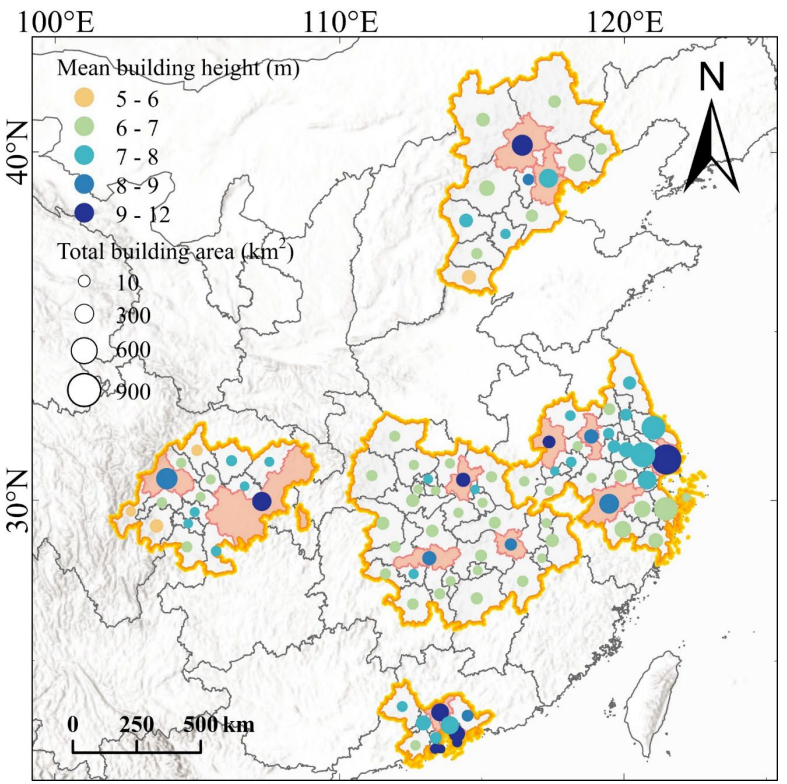
Name	Institution	Poster title	Contribution including period of research
Zilu Li	AIR, CAS	Integrating SDGSAT-1 with Sentinel-1/2 data for High-Resolution Building Height Estimation with a Deep Learning Framework	• Developed a deep learning model for building height estimation using Sentinel-1/2 and SDGSAT-1 data • September 2025-present
Muhammad Fahad Baqa	AIR, CAS	Investigating heat-related health risks related to local climate zones using SDGSAT-1 high-resolution thermal infrared imagery in an arid megacity	• Developed a thermal infrared remote sensing data processing approach and performed urban heat risk spatial evaluation using remote sensing and socioeconomic data • September 2025-present
Xuting Liu	AIR, CAS	Assessing urban sustainability in the Belt and Road region: a city-level analysis of SDG 11 indicators using earth observations	• Monitoring and assessing change trajectory of SDG 11 indicators in the Belt and Road region using Earth observation data • March 2025-present

Overview of Chinese YSs research

Overview of Chinese YSs research (when applicable)

- Building height is a vital vertical representation of urban morphology and is closely linked to the development of sustainable cities. However, accurately mapping building heights at a fine scale presents ongoing difficulties.
- This study developed a deep learning network using multi-modal Earth observation (EO) data for accurate building height estimation at 10-meter resolution, explored the importance of nighttime light data and its resolution in height estimation, and elucidated 3D urban morphology of the regions with the highest urbanization level in China.

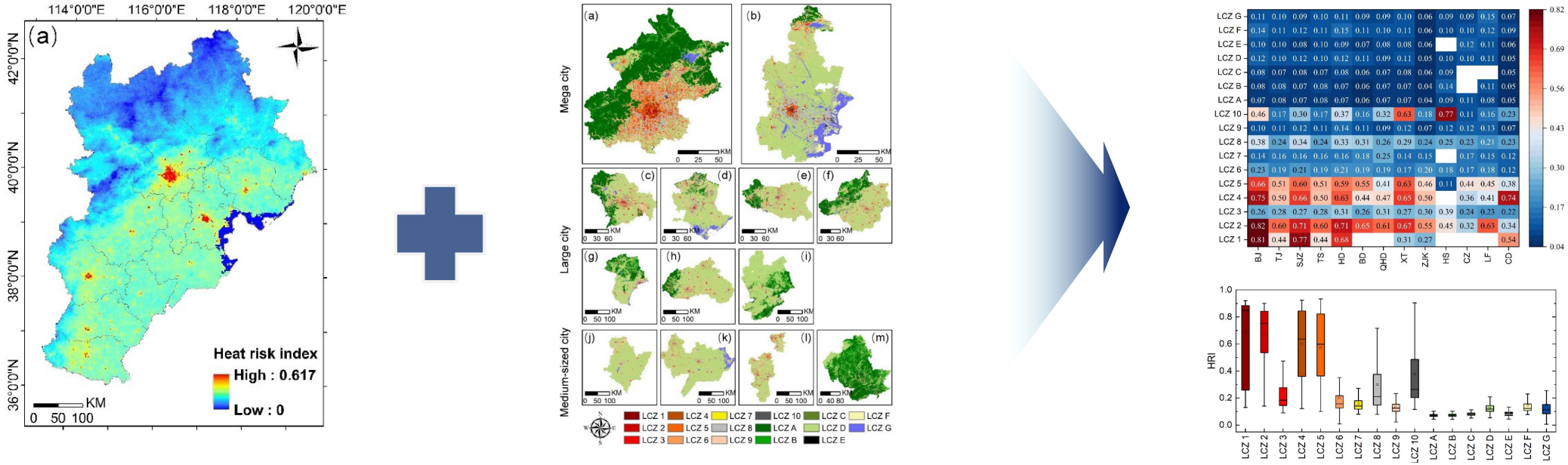




Overview of Chinese YSs research

Overview of Chinese YSs research (when applicable)

- Comprehensive heat risk assessment is crucial for providing targeted climate information and services to enhance cities' adaptation and mitigation capacities. However, the spatial resolution of administrative-level heat health risk assessments is inadequate for identifying intra-urban risk variations.
- This study developed a risk assessment framework for heat-related health risks integrating hazard, exposure, susceptibility, and adaptability factors at grid scale utilizing geospatial big data such as downscaled remote sensing data, disaggregated socioeconomic data and VGI data.

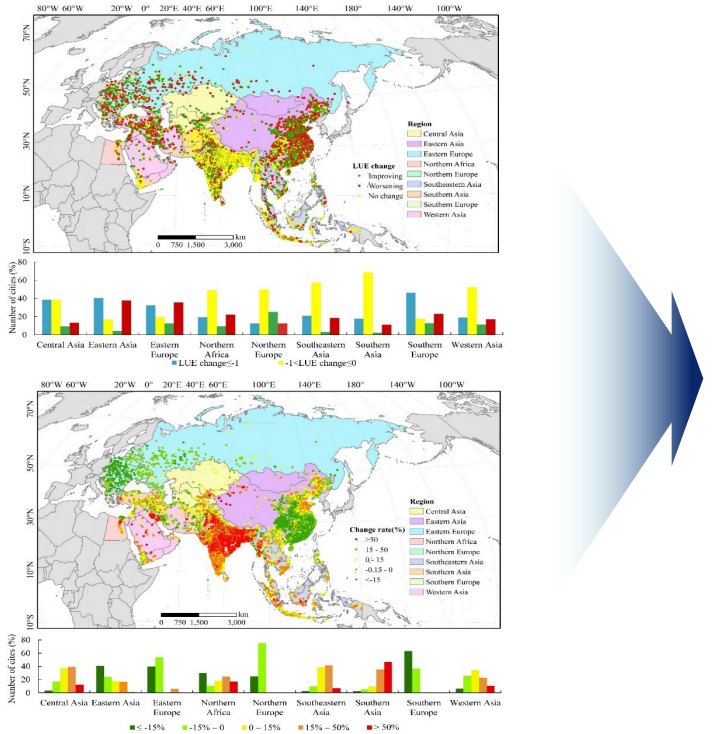


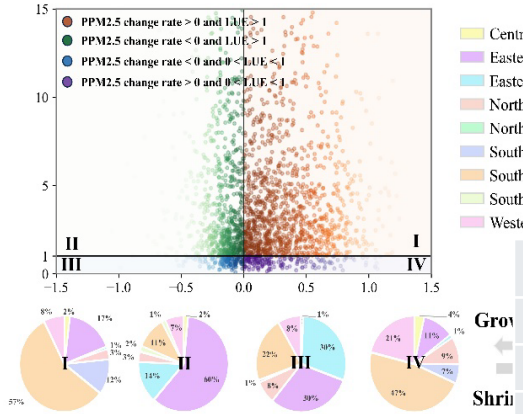
Baqa, M. F., Lu, L., Guo, H., Song, X., Alavipanah, S. K., Nawaz-ul-Huda, S., . . . Chen, F. (2025). Investigating heat-related health risks related to local climate zones using SDGSAT-1 high-resolution thermal infrared imagery in an arid megacity. *International Journal of Applied Earth Observation and Geoinformation*, 136, 104334.

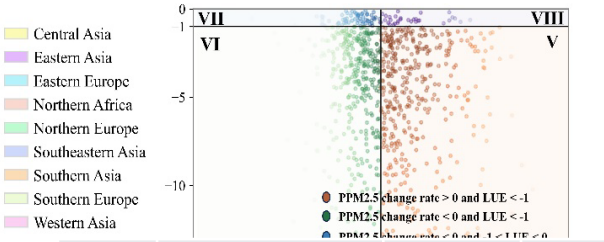
Overview of Chinese YSs research

Overview of Chinese YSs research (when applicable)

- The United Nations (UN) Sustainable Development Solutions Network (SDSN) strongly advocates for city-level reporting, emphasizing the crucial role of local and regional governments in implementing transformative actions.
- Leveraging Earth observation (EO) data, the joint research team analyzed the spatiotemporal dynamics of two urban SDG indicators—11.3.1 (Land Use Efficiency, LUE) and 11.6.2 (population-weighted $PM_{2.5}$ concentrations, $PPM_{2.5}$) in more than 7000 Belt and Road cities from 2000 to 2020.







Class	LUE	$PPM_{2.5}$	Proportion	Main distribution region
I	Sprawling growth	Increase	38.2%	South Asia (57%)
II	Sprawling growth	Decrease	22.6%	East Asia (60%)
III	Compact growth	Decrease	3.8%	Eastern Europe (30%), East Asia (30%)
IV	Compact growth	Increase	1%	South Asia (47%)
V	Moderate shrinking	Increase	15.3%	South Asia (37%), East Asia (33%)
VI	Moderate shrinking	Decrease	12.4%	East Asia (57%)
VII	Severe shrinking	Decrease	1.78%	Eastern Europe (52%)
VIII	Severe shrinking	Increase	1%	South Asia (34%), North Africa (24%), West Asia (21%)

Liu, X., Lu, L., Guo, H., Melchiorri, M., Hafner, S., Ban, Y., . . . Baqa, M. F. (2025). Assessing urban sustainability in the Belt and Road region: a city-level analysis of SDG 11 indicators using earth observations. *International Journal of Digital Earth, 18*(1), 2522395. doi:10.1080/17538947.2025.2522395

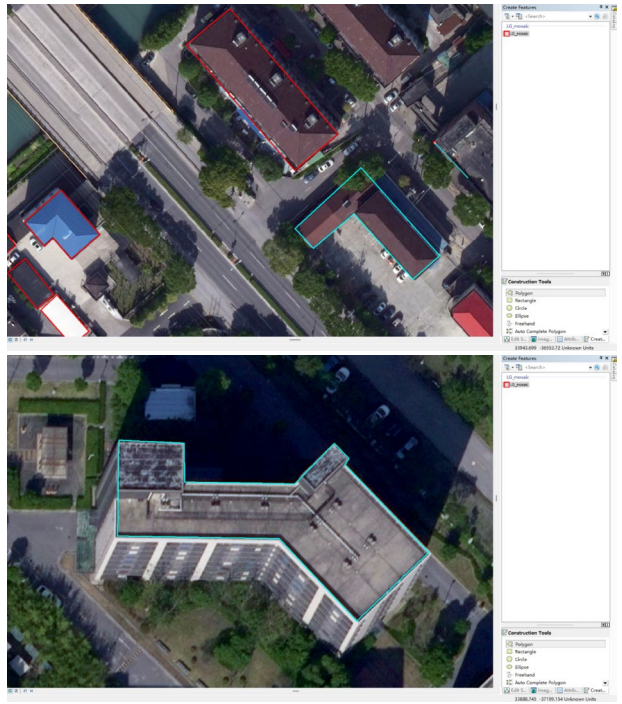
Chinese Young Scientists contributions in Dragon 6

Name	Institution	Poster title	Contribution including period of research
Shuwei Tang	East China Normal University	Poly-BRBLE: A Boundary Refinement Based Individual Building Localization and Extraction Model Combined with Regularization	Experiment Conduction Paper Writing
Renjie Ji	East China Normal University		Experiment Conduction
Yuling Zhou	East China Normal University		Data Collection

Background and Objective

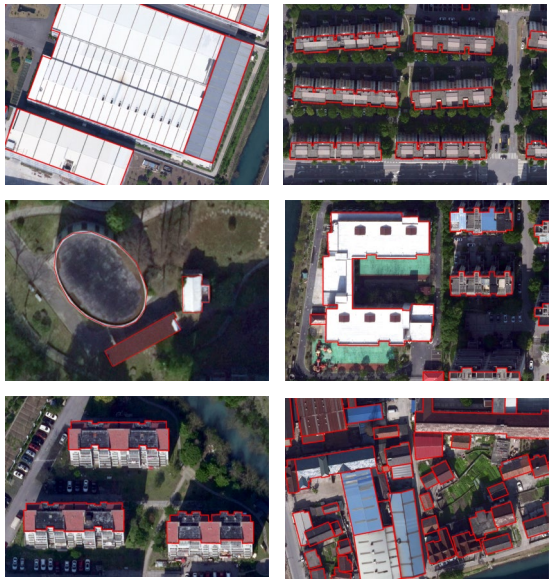
Due to the diversity of building structures, the complexity of urban environments, and the variability in remote sensing imaging conditions, achieving high-precision automated building vector mapping from remote sensing imagery is extremely challenging.

Reliance on Manually Annotated Building Vector Base Maps

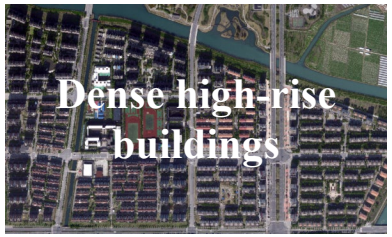


Difficulties Faced in Automated Building Extraction

Diversity of Building Structures



Complexity of Urban Environments





Variability in Remote Sensing Imaging Conditions





Background and Objective



中国科学技术交流中心
China Science and Technology Exchange Center

→ THE EUROPEAN SPACE AGENCY

Traditional Methods

- Machine Learning
- Threshold Segmentation
- Contour Evolution

↓

- Building Index
- Feature Extraction Operators
- ...
- Active Contour Model

MBI (Huang..., 2011)
NSBI、DSBI (Gu..., 2018)

Adaptability to complex environments

Semantic Segmentation

- FCN
- DeepLab
- U-Net
- Transformer

↓

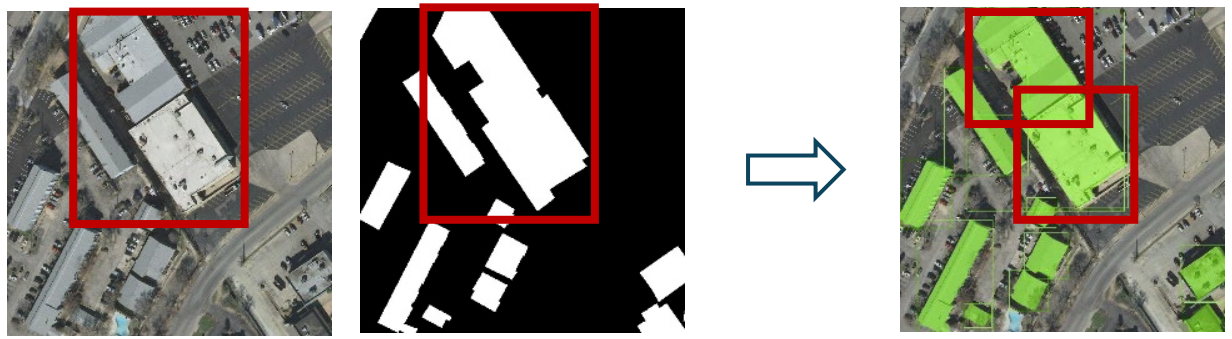
- Multi-scale
- Multi-angle
- Prone to Occlusion
- Prone to Confusion

↓

MAP-Net (Zhu..., 2020)
HiT (Zhang..., 2024)

Difficult to extract single buildings in low-density areas

Original | Semantic Segmentation | Instance Segmentation



Instance Segmentation Methods

- Mask RCNN
- SOLOv2
- HTC
- ...
- PointRend

↓

- Corner Regression
- Pixel Classification
- Regularized Post-processing

↓

OEC-RNN (Huang…, 2021)
PolyBuilding (Hu…, 2023)

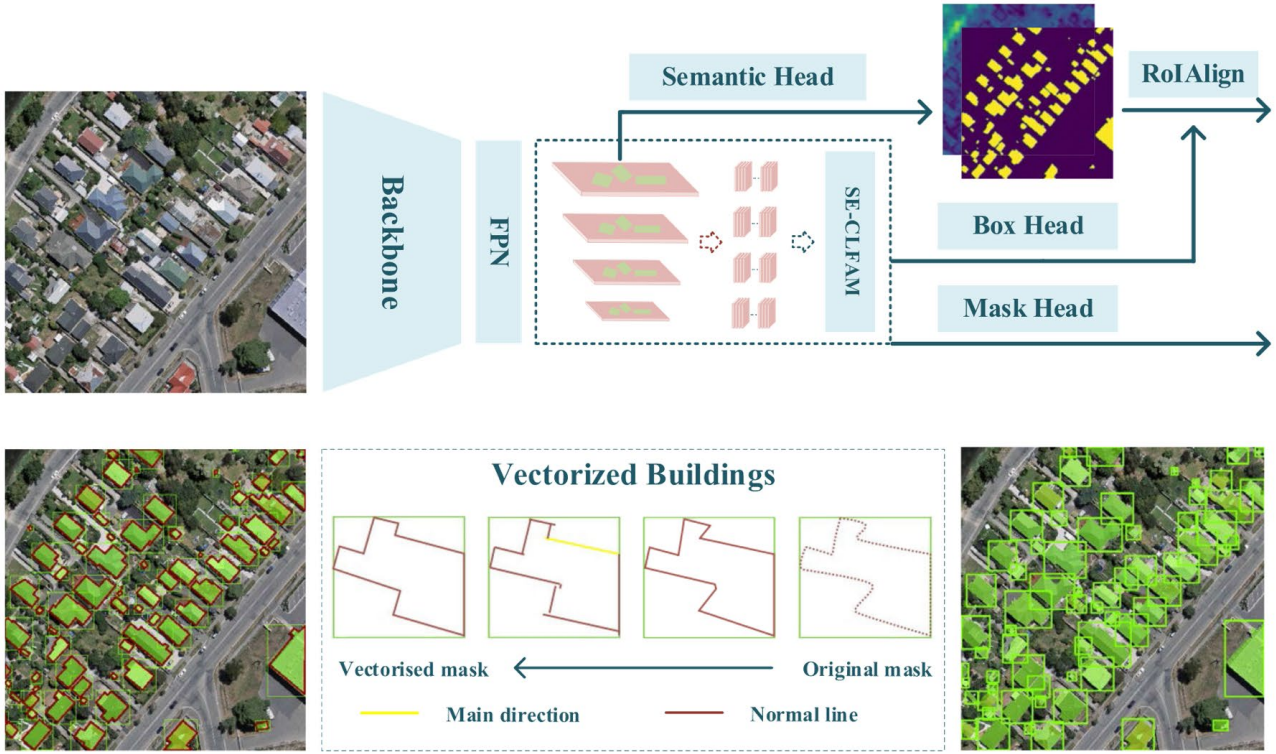
RefineMask (Zhang…, 2021)
DynaMask (Li…, 2023)

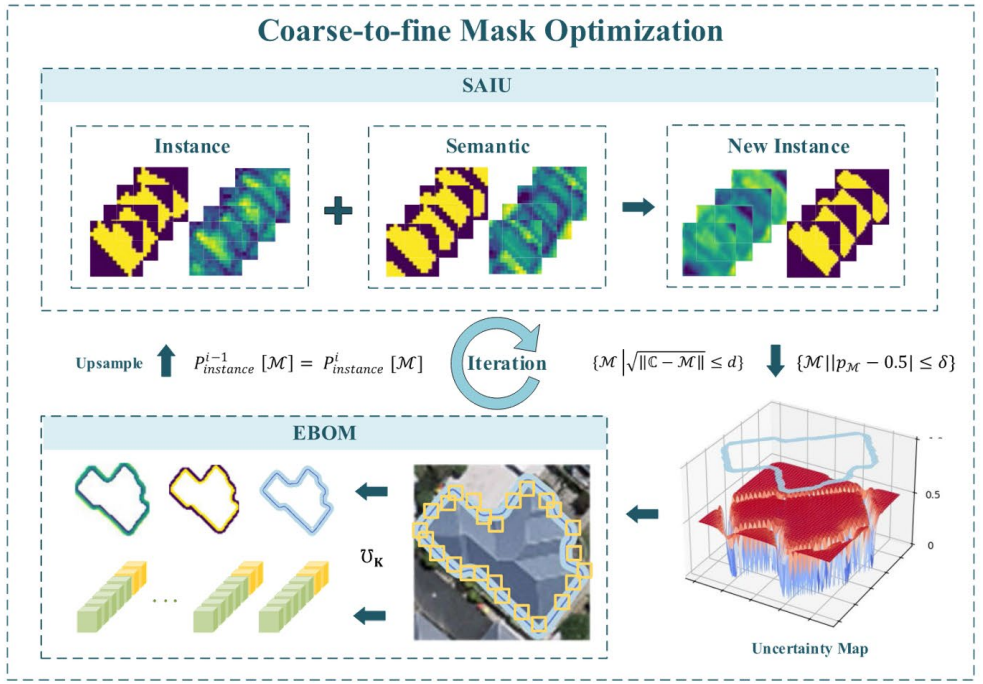
FFL (Girard..., 2021)
DF (Li..., 2023)

Successful in location and extraction of individual buildings but low mask quality and compliex model structure

Method

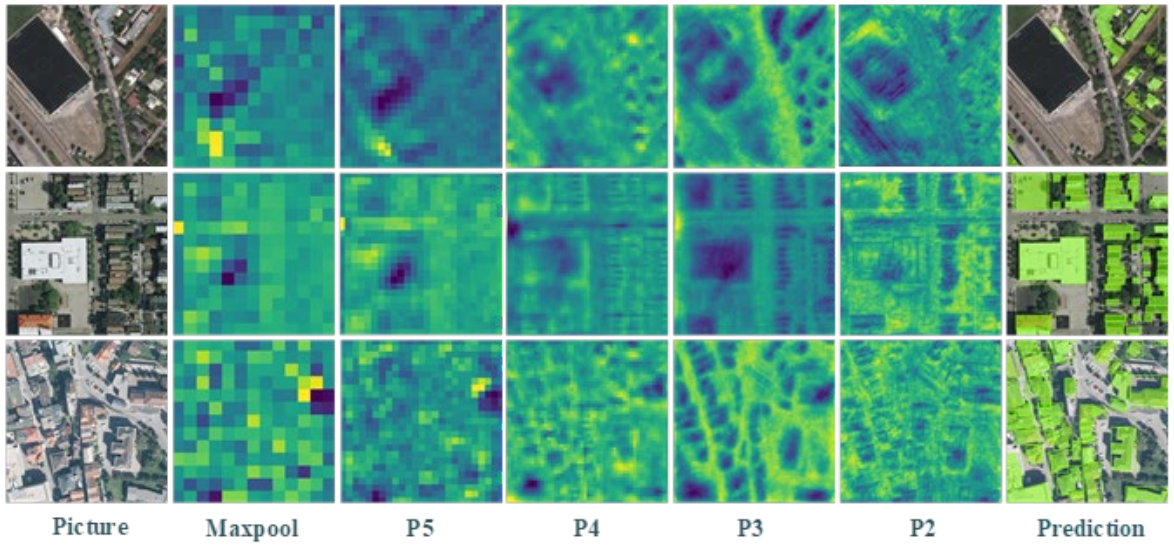
1. Integrate multi-feature layers to improve building detection in complex environments.
2. Refine edge details by analyzing geometric and probabilistic properties of "uncertain points" in buffer zones.
3. Regularize building masks by distinguishing between "cut lines" and true main direction lines to optimize the algorithm.

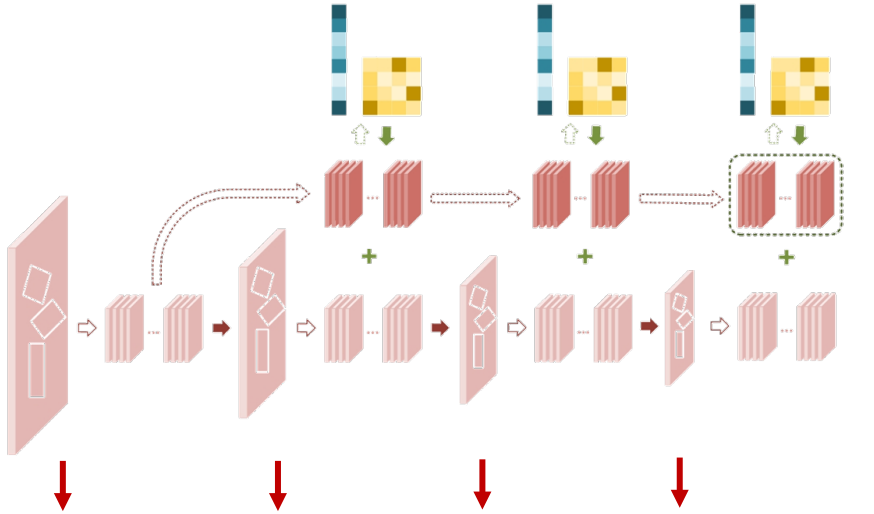




Method

Cross-Feature Layer Fusion & Propagation





$$n = \log_2(\sqrt{wh}/28)$$

Select specific feature layers

Fuse multi-scale feature layers

Channel attention mechanism

Sigmoid normalization

$$\mathcal{R}_i = \mathcal{R}_{i-1} + f_{se}(f_{de}([\mathcal{R}_{i-1}, \mathcal{R}_i])) \cdot f_{sigmoid}(f_{de}([\mathcal{R}_{i-1}, \mathcal{R}_i])) \cdot \mathcal{R}_i$$

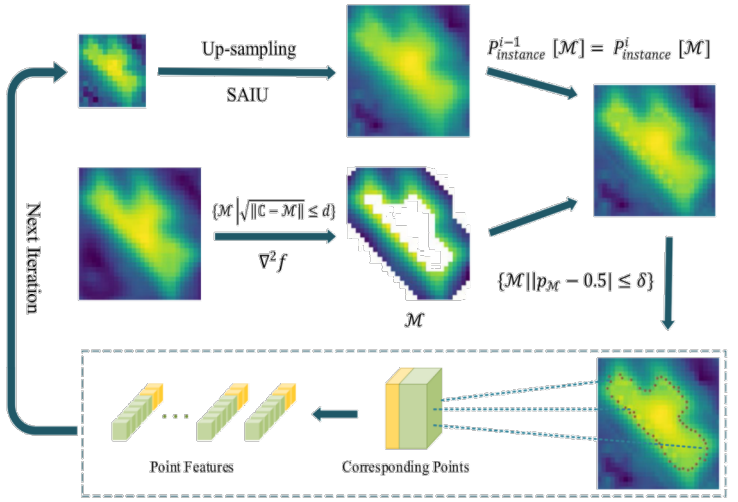
Interest Region Feature (Layer i)

Interest Region Feature (Layer i-1)

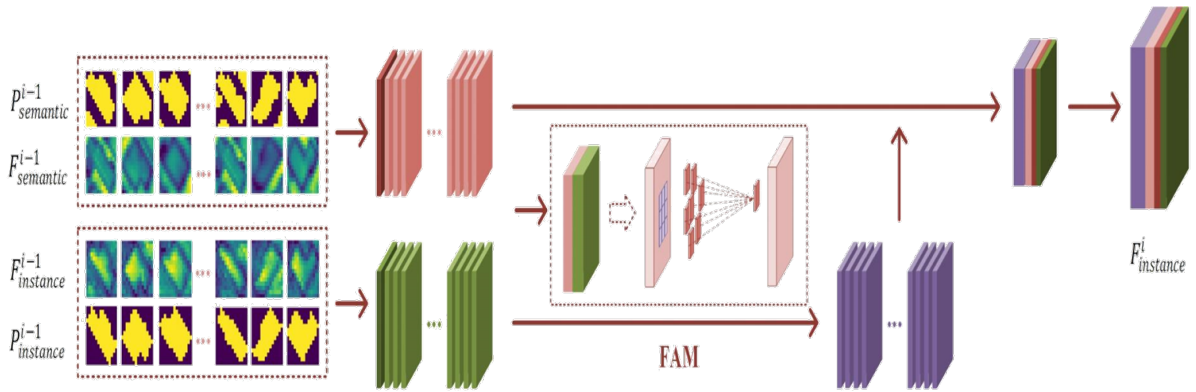
Feature dimensionality reduction

Method

Edge Optimization: Geometric & Probabilistic



Feature Scale Fixed



Algorithm 1 Coarse-to-Fine Mask Optimization

Input: initial instance features $F_{14\times14}$,
initial instance predictions $P_{14\times14}$,
semantic features $F_{semantic}$,
semantic predictions $P_{semantic}$,
mask proposals $Proposals_{mask}$

Output: the instance prediction map after coarse-to-fine mask optimization $P^{final}_{instance}$

Initialize: $F^{(0)}_{instance} = F_{14\times14}$, $P^{(0)}_{instance} = P_{14\times14}$,
$size_{initial} = 14$, $size_{final} = 112$

While $size \le 112$ **do**
- $F^{i}_{instance}, P^{i}_{instance} = SAIU(F^{i-1}_{instance}, P^{i-1}_{instance}, F_{semantic}, P_{semantic})$;
- Extract the boundary area $\mathcal{M}$ of $P^{i}_{instance}$ by the Laplace Operator;
- Up-sample $P^{i-1}_{instance}$;
- $P^{i-1}_{instance}[\mathcal{M}] = P^{i}_{instance}[\mathcal{M}]$;
- $P_{fuse} = P^{i-1}_{instance}$;
- Select $4K$ points from P_{fuse} to form ψ, and the corresponding features denoted as $\mho_K$;
- $P_{fuse}[\psi] = MLP(\mho_K)$;
- $P^{i}_{instance} = P_{fuse}$;
- $size = size \times 2$;

End While

Return $P^{final}_{instance} \leftarrow P^{i}_{instance}$

Experiments

WHU Aerial Building Dataset

	AP_{box}	AP_{mask}	AP^{50}_{mask}	AP^{75}_{mask}	AP_s	AP_m	AP_l	AR_{mask}	AR_s	AR_m	AR_l
Mask RCNN	70.8	67.8	91.9	79.8	55.9	79.5	60.5	72.1	62.8	82.9	73.2
SOLOV2	-	66.1	89.1	76.7	51.3	81.0	70.0	70.6	58.1	84.9	87.8
YOLACT	53.4	49.9	75.7	58.6	32.8	68.1	45.2	55.3	38.9	74.3	62.8
HTC	72.2	69.8	91.8	81.8	58.3	81.1	66.0	74.1	65.3	84.2	78.5
PointRend	71.8	68.0	91.9	80.0	55.7	80.1	65.3	72.0	62.0	83.6	78.9
RefineMask	71.7	70.1	92.0	81.2	57.9	82.3	66.1	74.3	64.5	85.7	80.0
CATNet	72.3	68.7	91.9	79.9	56.1	80.7	65.1	73.1	63.4	84.3	76.4
BSPM	59.3	52.7	83.0	62.0	39.8	67.2	38.9	57.2	44.4	72.2	54.4
BRBLE	**73.2**	**72.1**	**93.0**	**83.3**	**60.3**	**83.5**	**71.3**	**76.6**	**67.5**	**87.1**	**82.3**

Chinese Typical Urban Building Dataset

	AP_{box}	AP_{mask}	AP^{50}_{mask}	AP^{75}_{mask}	AP_s	AP_m	AP_l	AR_{mask}	AR_s	AR_m	AR_l
Mask RCNN	47.4	43.7	70.6	48.4	17.0	49.7	55.5	56.6	34.1	62.6	66.4
SOLOV2	-	45.6	72.2	50.0	16.3	52.2	59.7	60.1	31.9	66.9	74.8
YOLACT	35.6	33.7	61.7	33.9	9.5	39.7	41.9	48.0	26.0	53.9	57.3
HTC	48.8	44.8	70.3	49.2	17.0	50.8	58.3	**60.8**	**39.9**	66.0	71.0
PointRend	48.2	44.1	71.0	48.9	16.6	50.3	57.0	56.2	32.1	62.4	67.6
RefineMask	48.2	46.0	72.1	50.8	18.2	51.8	59.7	58.5	34.7	64.5	70.0
CATNet	47.4	43.9	70.4	47.9	17.2	49.6	56.7	56.7	34.0	62.3	68.3
BSPM	30.9	26.9	55.1	24.5	11.4	33.7	28.9	38.2	20.0	44.4	41.0
BRBLE	**49.7**	**47.5**	**73.1**	**52.6**	**19.4**	**53.1**	**61.5**	60.7	38.5	**66.1**	**72.5**

Inria Polygon Building Dataset

	AP_{box}	AP_{mask}	AP^{50}_{mask}	AP^{75}_{mask}	AP_s	AP_m	AP_l	AR_{mask}	AR_s	AR_m	AR_l
Mask RCNN	47.1	45.5	72.7	51.1	32.5	56.7	45.2	54.6	41.4	65.9	62.7
SOLOV2	-	43.0	70.7	47.6	27.7	55.7	51.1	52.3	35.4	66.2	69.8
YOLACT	31.8	28.4	55.7	26.4	19.0	36.4	34.9	37.1	25.4	46.7	49.6
HTC	48.6	46.1	72.7	52.4	33.7	56.8	48.9	55.2	42.3	66.0	65.0
PointRend	48.7	45.8	73.6	51.8	32.9	56.8	49.9	54.2	40.8	65.5	64.7
RefineMask	49.0	47.9	74.5	54.4	34.4	59.3	51.9	56.7	42.7	68.5	67.1
CATNet	48.8	46.6	74.0	52.4	33.3	57.8	48.7	55.7	42.2	67.3	64.2
BSPM	25.6	23.6	48.8	20.8	17.6	31.0	14.0	33.8	24.1	43.1	26.7
BRBLE	**50.2**	**49.1**	**75.1**	**55.9**	**35.7**	**60.5**	**53.9**	**58.1**	**44.4**	**69.6**	**68.1**

Custom SH Building Dataset

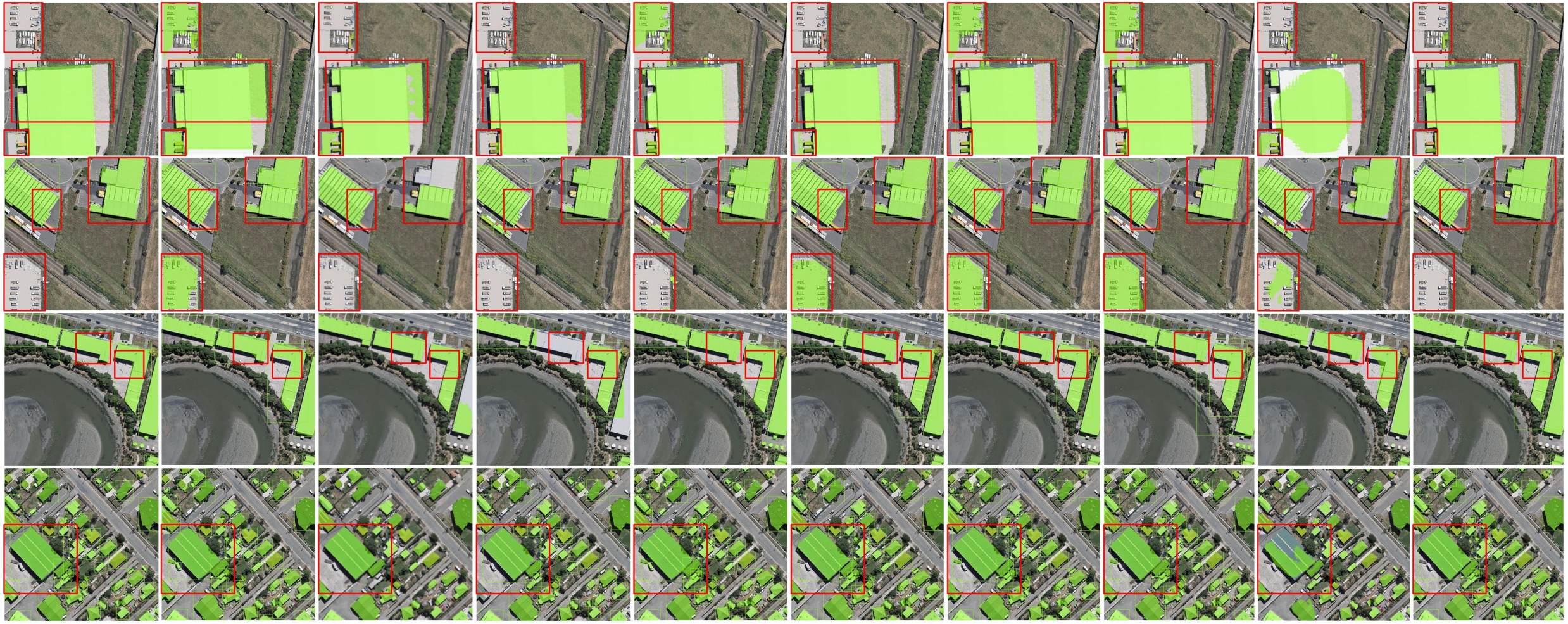
	AP_{box}	AP_{mask}	AP^{50}_{mask}	AP^{75}_{mask}	AP_s	AP_m	AP_l	AR_{mask}	AR_s	AR_m	AR_l
Mask RCNN	65.6	59.3	83.6	70.3	29.1	64.6	69.9	65.9	40.6	70.9	76.3
SOLOV2	-	52.2	75.4	59.7	12.1	56.8	72.4	60.2	21.7	65.6	81.3
YOLACT	40.1	34.8	60.1	37.4	3.8	39.4	49.1	43.3	9.7	48.2	61.2
HTC	68.1	61.5	83.8	72.6	28.9	66.6	73.7	67.5	40.2	72.7	79.1
PointRend	67.2	60.9	84.5	71.7	29.5	65.4	75.1	66.6	38.3	71.4	80.3
RefineMask	66.7	65.1	85.0	74.8	33.1	70.0	77.3	70.7	44.9	75.1	82.8
CATNet	69.1	62.6	85.6	73.3	34.0	67.3	73.2	69.2	45.4	73.6	79.7
BSPM	33.4	28.4	55.2	27.7	6.0	34.6	34.8	36.3	10.3	41.6	46.6
BRBLE	**70.3**	**68.5**	**86.4**	**78.1**	**37.7**	**72.8**	**81.1**	**74.1**	**49.4**	**78.2**	**86.2**

1. Model performs best on high-quality images.

2. Applicable to various building scales; most significant boundary improvement for large targets.

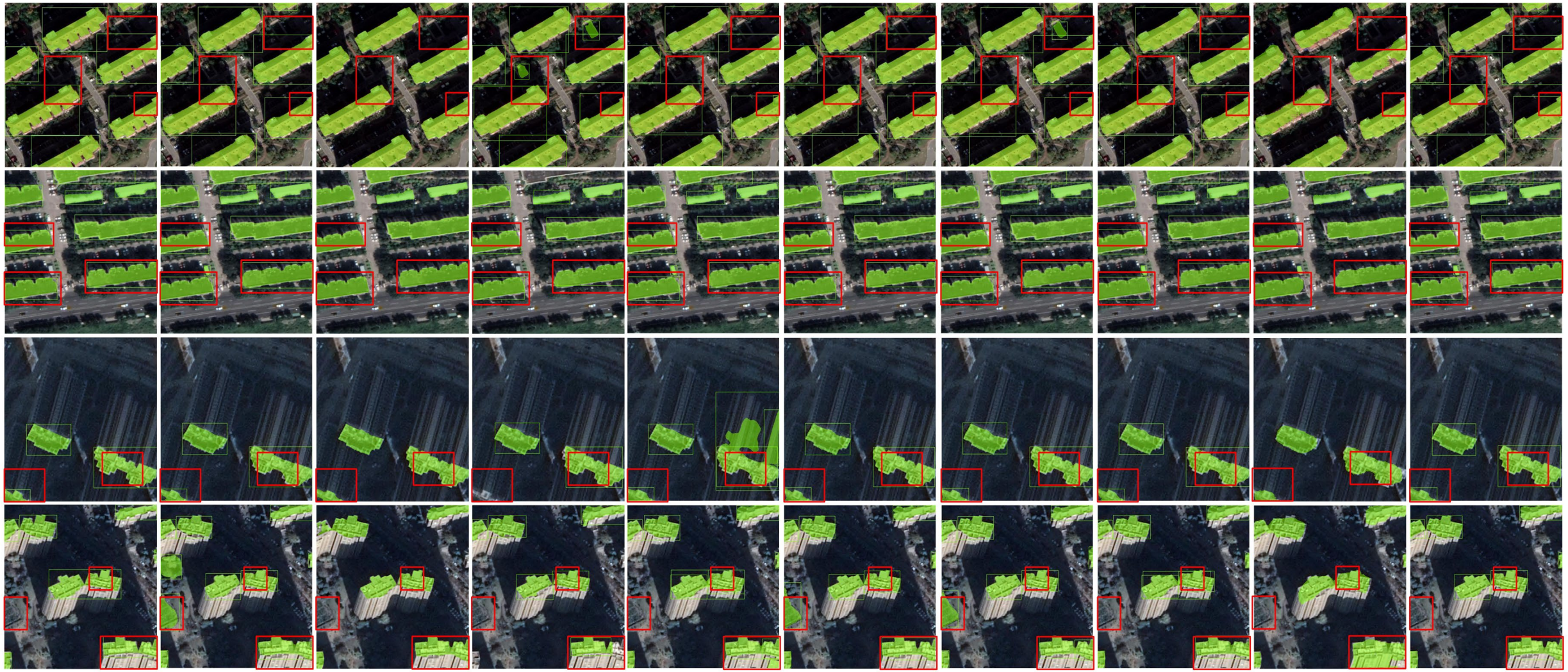
Experiments

WHU Aerial Building Dataset



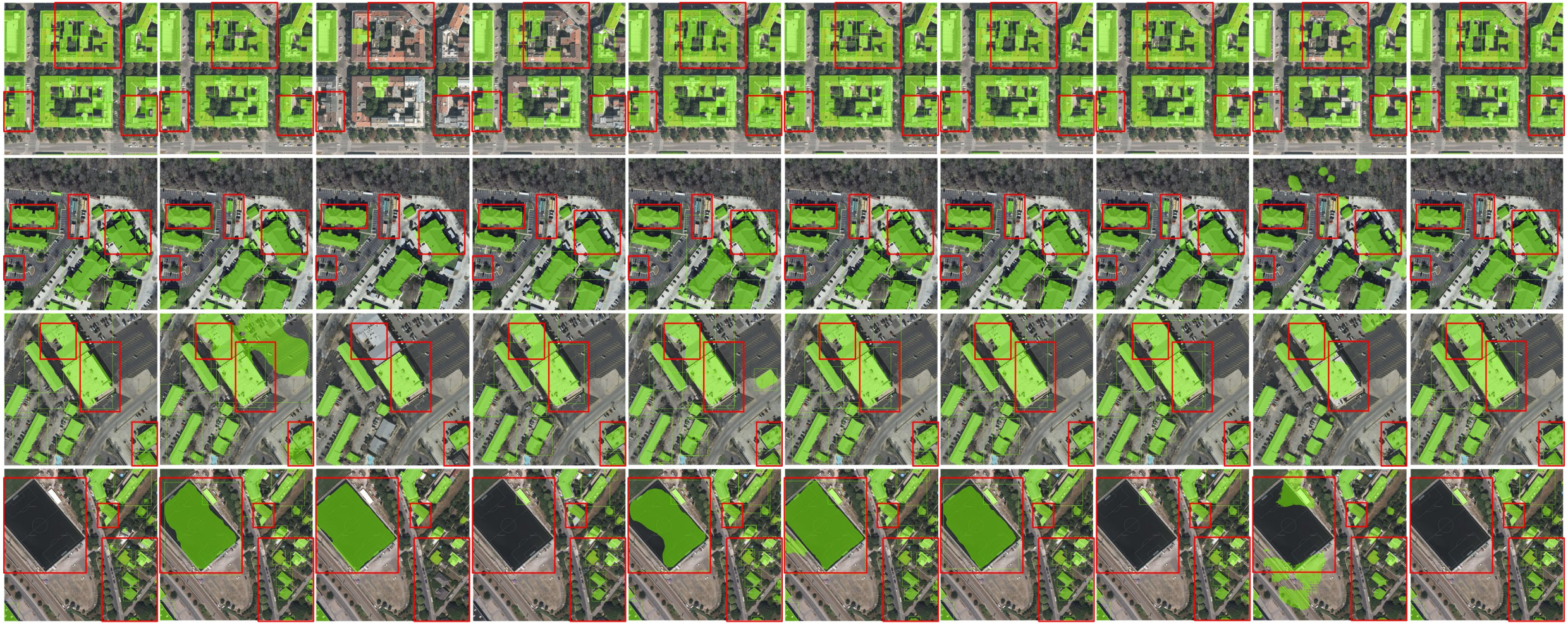
Experiments

Chinese Typical Urban Building Dataset



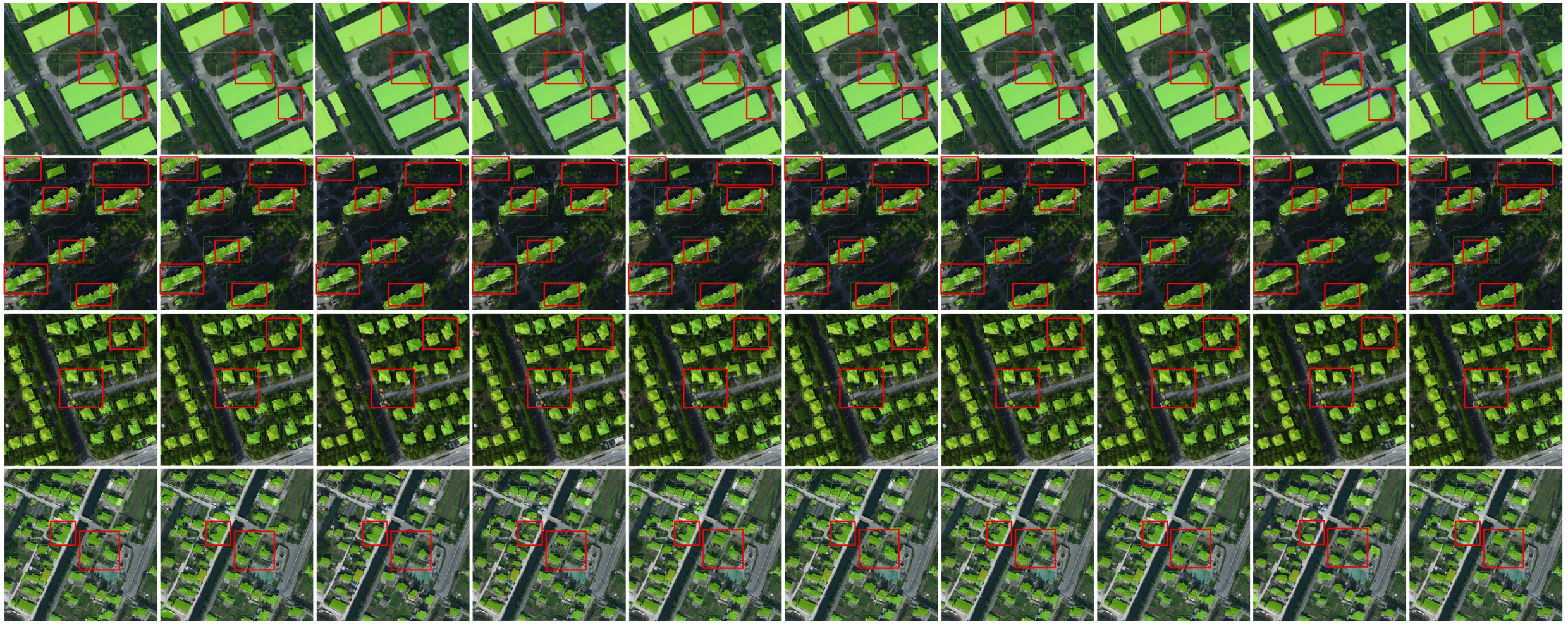
Experiments

Inria Polygon Building Dataset



Experiments

Custom SH Building Dataset



Experiments

Computational Efficiency Comparison

Method	*Params* (*M*)	*Flops* (*G*)	Inference Time (ms)
MaskRCNN	62.97	168.20	36.4
SOLOV2	65.22	225.29	44.2
YOLACT	**53.72**	**84.727**	**31.3**
HTC	99.20	1717.85	55.1
Point Rend	74.70	168.20	37.5
RefineMask	63.89	262.58	50.3
CATNet	72.51	254.00	69.9
BSPM	40.19	133.65	49.4
BRBLE	63.21	186.44	88.5

The multi-scale feature fusion and propagation module and the building edge optimization structure introduce more feature layers, increasing parameter count and computational complexity. This is further amplified by the two-step geometric and probabilistic correction process in the latter.

Experiments

Regularization Accuracy Comparison: SH Building Dataset

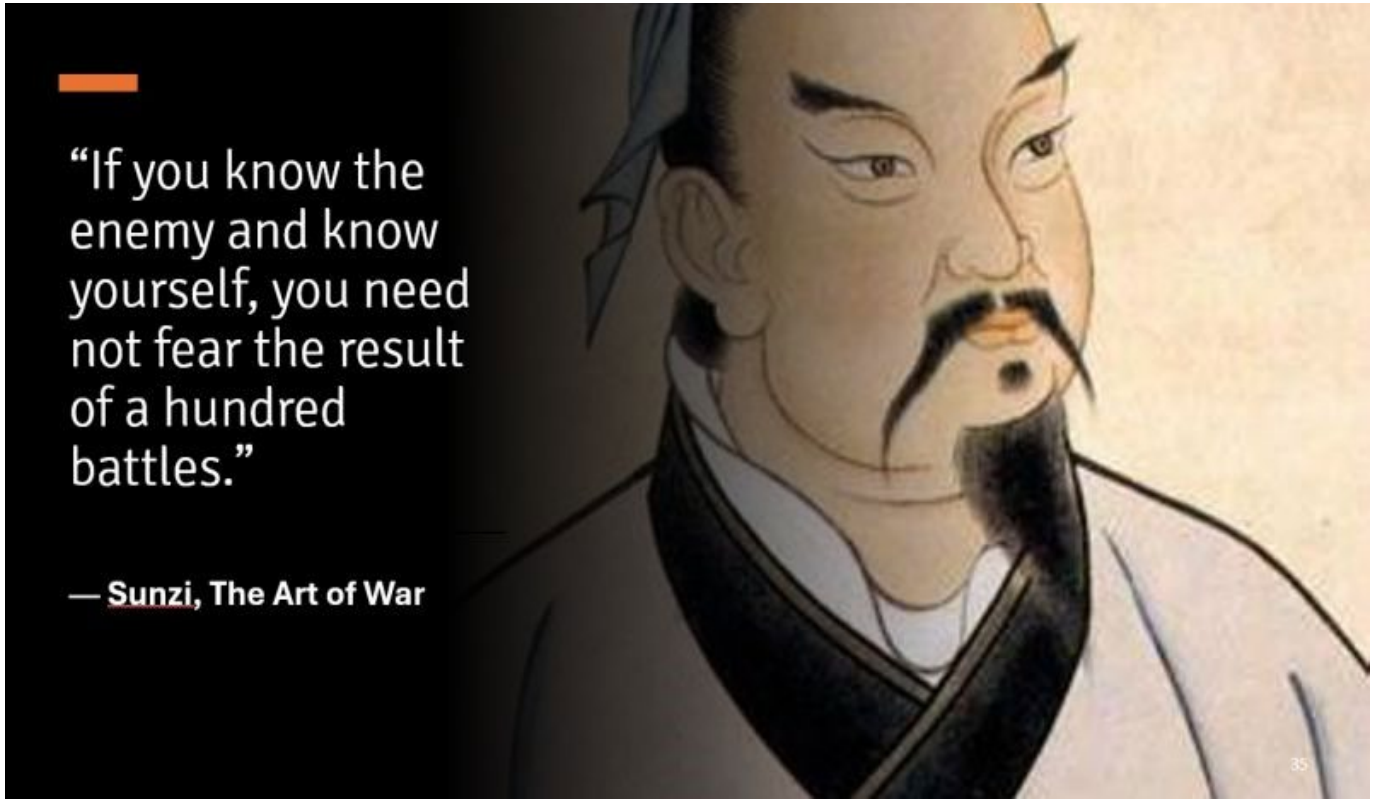
Methods	AP_{mask}	AP^{50}_{mask}	AP^{75}_{mask}	AP_s	AP_m	AP_l	AR_{mask}	AR_s	AR_m	AR_l
Poly-Mask RCNN	53.6	80.3	63.8	22.9	58.6	64.6	59.9	32.0	65.2	71.8
Poly-SOLOV2	44.2	63.2	53.5	4.8	49.3	65.7	49.2	6.2	54.9	73.3
Poly-YOLACT	29.0	48.8	32.9	1.3	32.1	45.7	34.7	2.0	38.1	54.9
Poly-HTC	53.7	78.2	64.6	21.2	59.2	66.8	59.9	28.4	65.6	73.9
Poly-PointRend	55.8	81.1	66.0	25.5	60.9	67.9	61.7	32.9	66.9	74.7
Poly-RefineMask	57.8	81.0	69.1	26.0	63.3	69.4	63.6	34.9	68.9	76.3
Poly-CATNet	55.9	81.6	66.8	26.9	60.5	67.1	62.4	35.8	67.3	74.2
Poly-BSPM	26.0	54.0	22.8	4.6	31.5	32.4	33.7	8.5	38.4	44.7
Poly-BRBLE	**60.4**	**82.4**	**71.5**	**29.9**	**65.4**	**72.6**	**66.3**	**38.3**	**71.3**	**79.0**

Chinese Young Scientists contributions in Dragon 6

Name	Institution	Poster title	Contribution including period of research
Furong Zhang	USTB	-	Build system dynamics models for city repairing, 2024-2026
Yian Zhu	USTB	-	Spatiotemporal casualty assessment modeling, 2024-2027

Objective

- To enhance urban resilience and mitigate the impact of potential risks to cities, it is important to gain a comprehensive understanding of risks, including both those that have already occurred and those that may occur in the future.
- Therefore, it is necessary to develop effective AI-driven urban sening and monitoring and disaster simulation methods.



"知己知彼，百战不殆。"
——孙武，《孙子兵法》

Objective

- The research group at the University of Science and Technology Beijing, led by Prof. Zhen Xu, focuses on the impacts of natural disasters on urban systems.
- Accurate urban sensing and disaster simulation results can support decision-making and urban planning by government agencies.



Urban sensing and monitoring
(occurred)



Disaster simulation
(may occur)



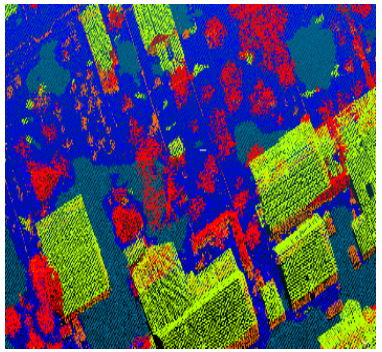
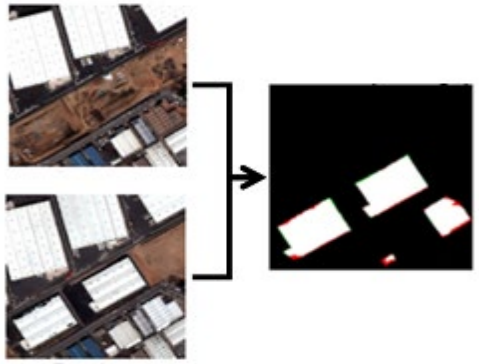
Decision making



Urban planning

Objective: Urban Sensing and Monitoring

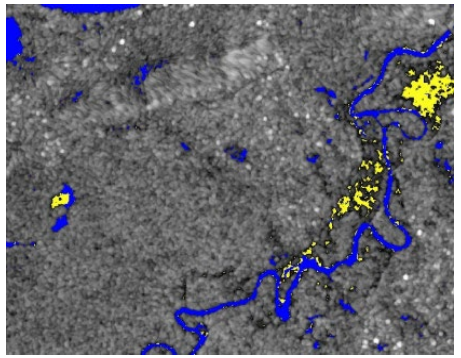
- Develop deep learning-based methodologies (change detection, land use classification, etc.) for urban sensing and monitoring.

Buidling extraction and change detection



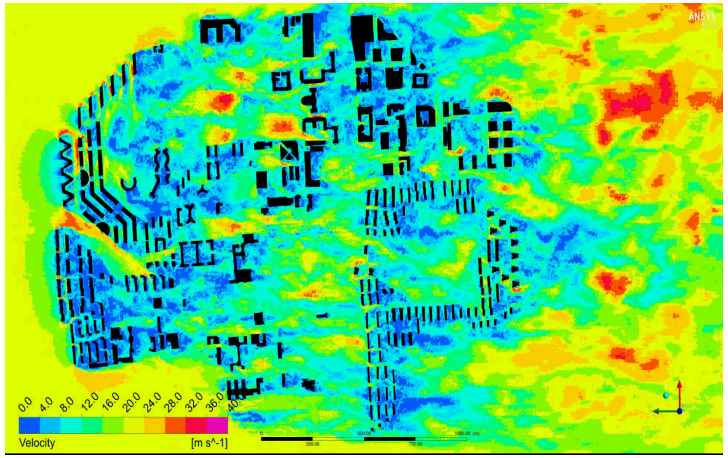

Infrastructure monitoring

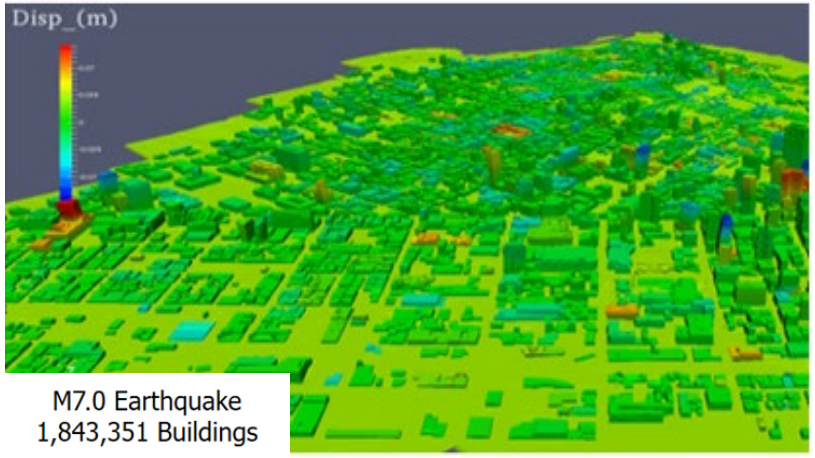
Urban disaster assessment

Objective: Urban Disaster Simulation

- Develop simulation methodologies for extreme weather events and natural hazards.
- City-scale earth observation data and corresponding shapefiles serve as the foundation for physical simulation models.



Wind disaster



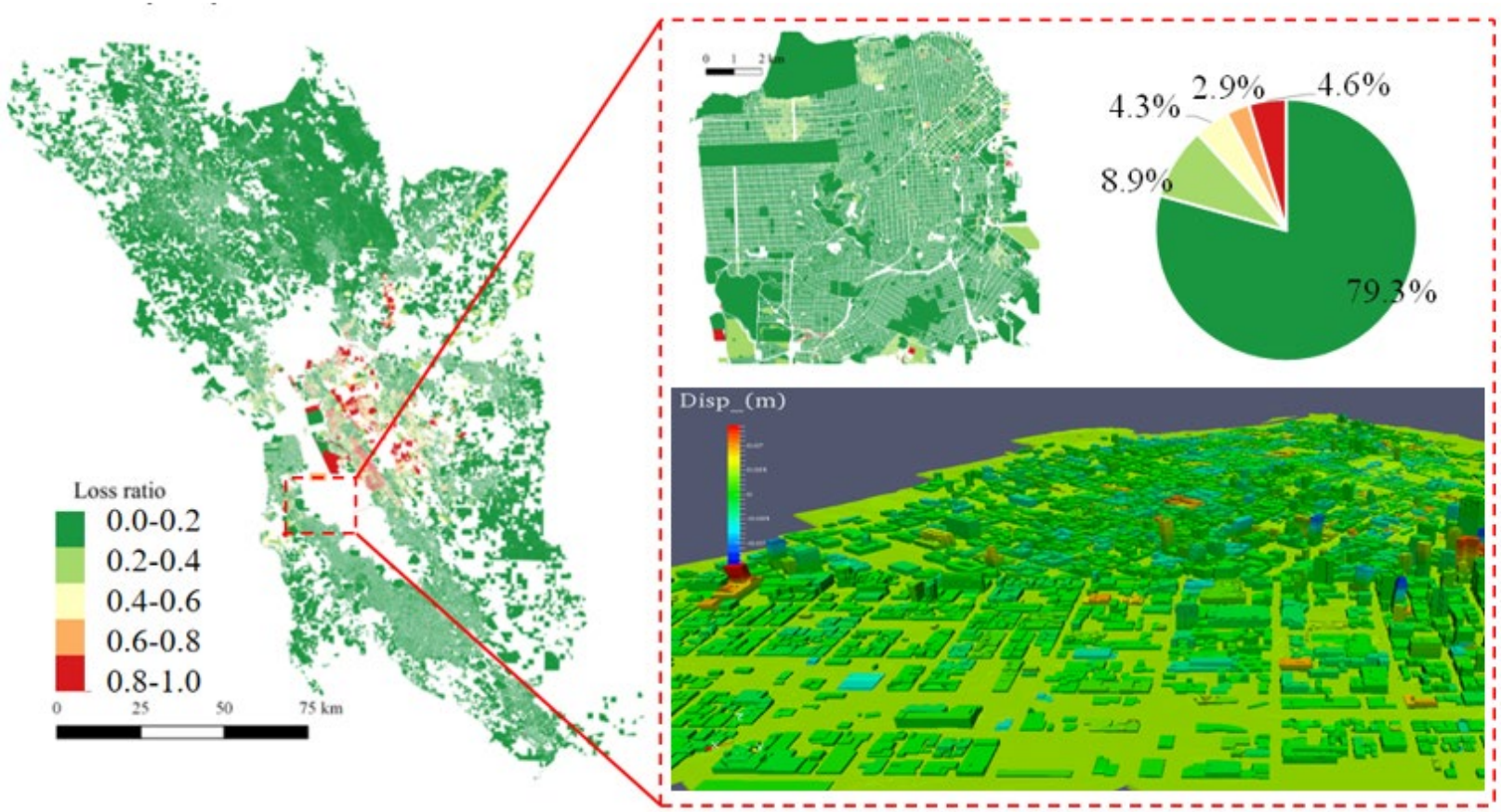
Earthquake



Fire

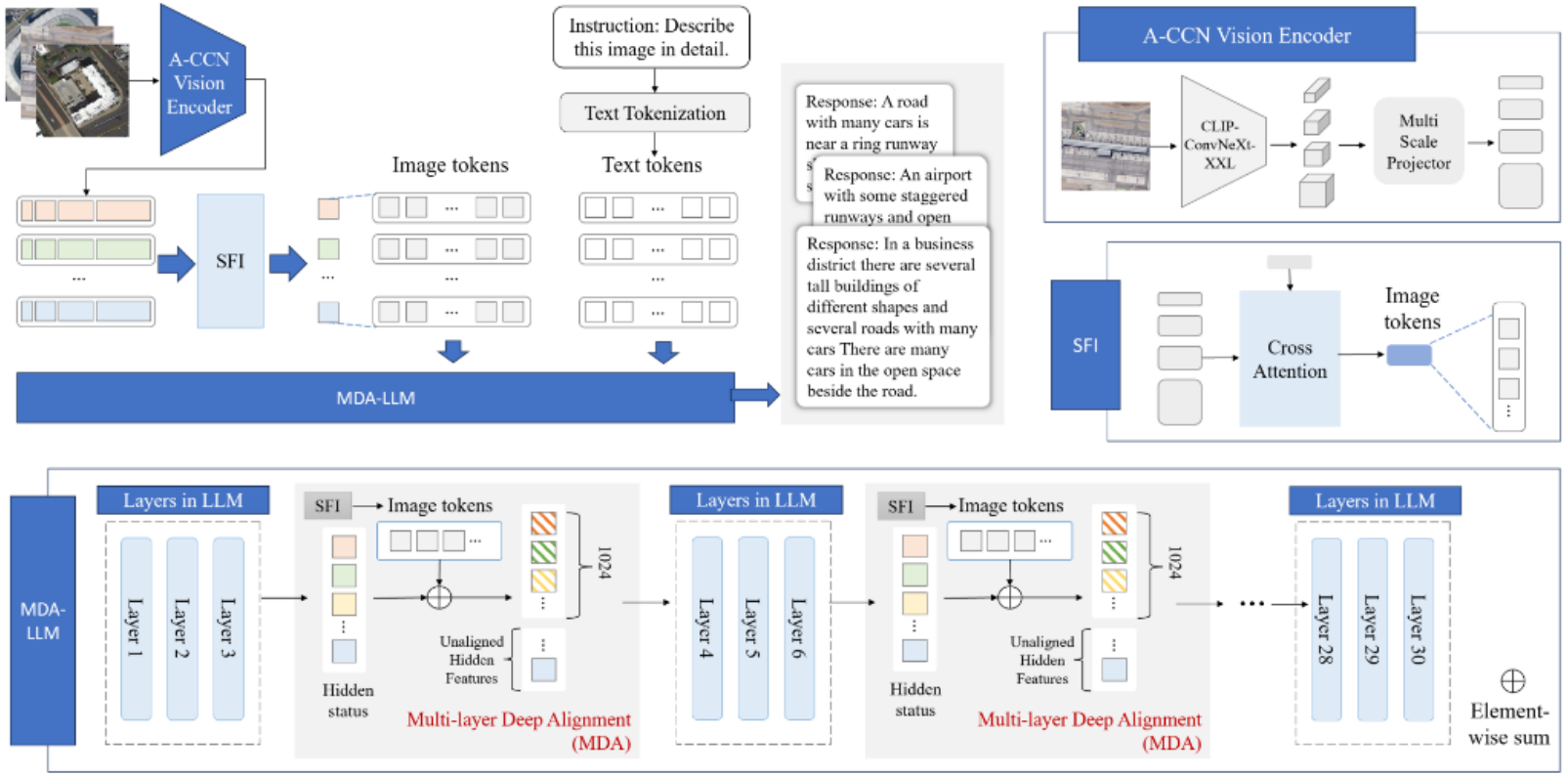
Objective: Urban Disaster Simulation

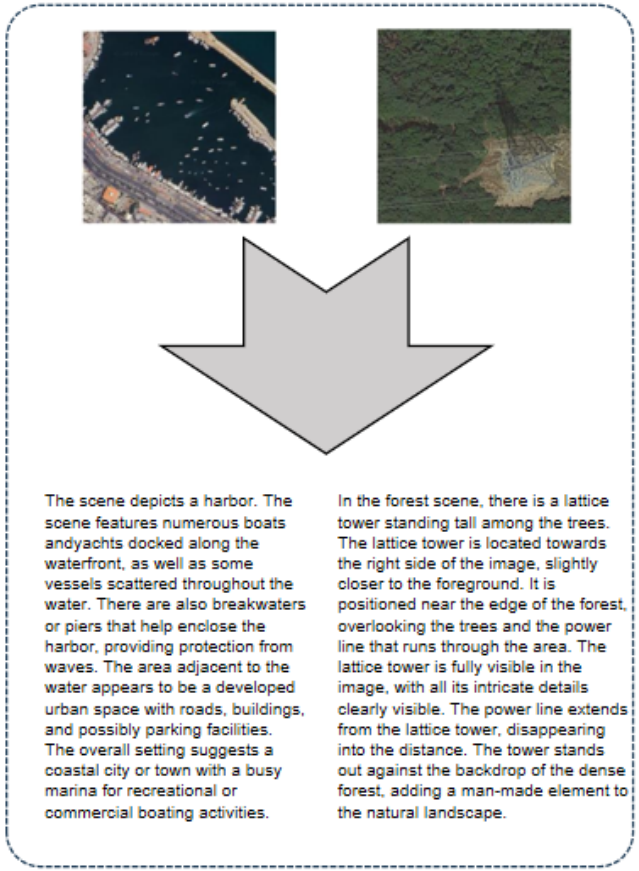
- Develop simulation methodologies for extreme weather events and natural hazards.
- City-scale earth observation data and corresponding shapefiles serve as the foundation for physical simulation models.



Results Reporting: Urban Sensing and Monitoring

- A visual-language model for remote sensing scene understanding, generating descriptive text from input optical images.





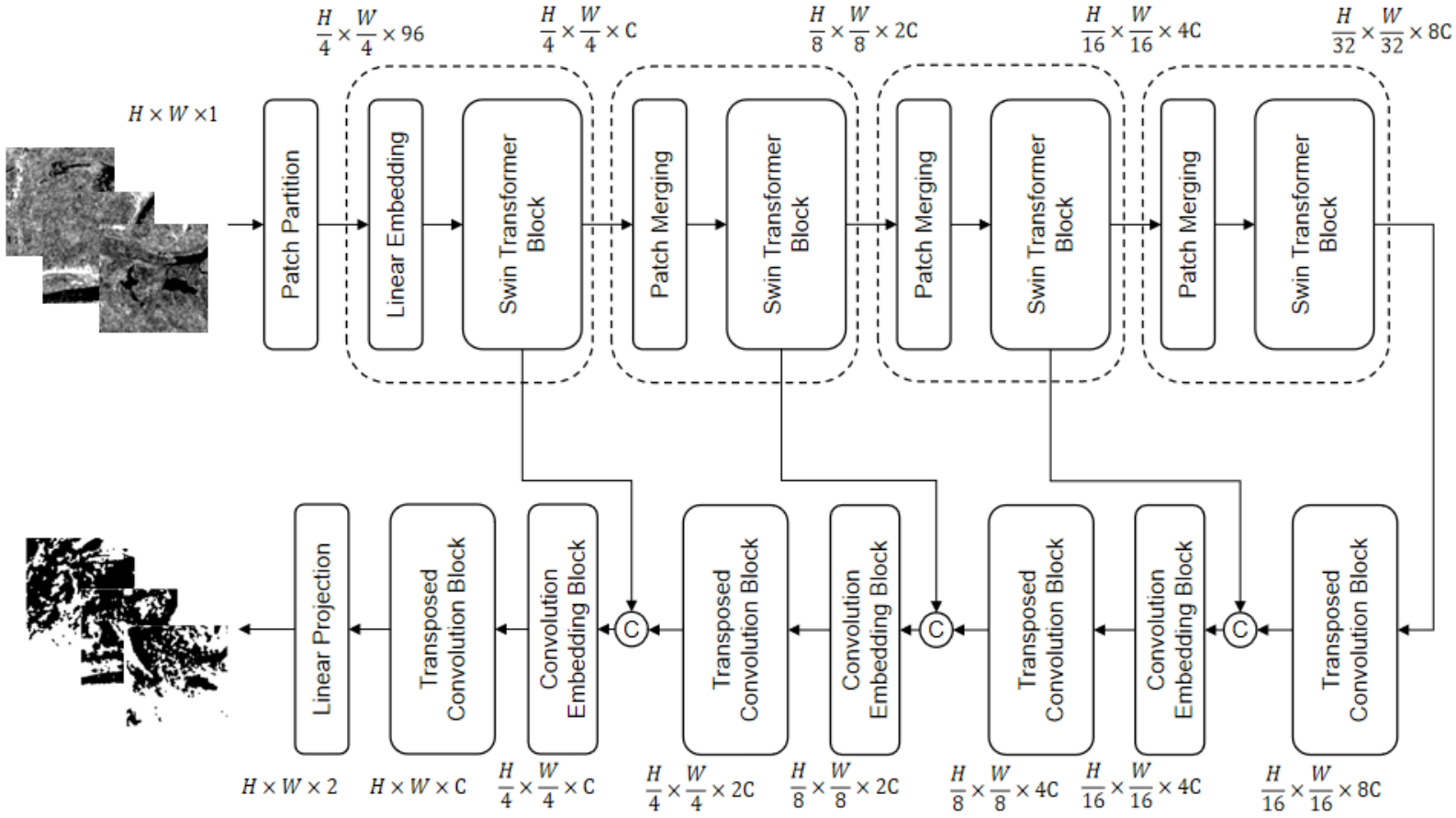
The scene depicts a harbor. The scene features numerous boats andyachts docked along the waterfront, as well as some vessels scattered throughout the water. There are also breakwaters or piers that help enclose the harbor, providing protection from waves. The area adjacent to the water appears to be a developed urban space with roads, buildings, and possibly parking facilities. The overall setting suggests a coastal city or town with a busy marina for recreational or commercial boating activities.

In the forest scene, there is a lattice tower standing tall among the trees. The lattice tower is located towards the right side of the image, slightly closer to the foreground. It is positioned near the edge of the forest, overlooking the trees and the power line that runs through the area. The lattice tower is fully visible in the image, with all its intricate details clearly visible. The power line extends from the lattice tower, disappearing into the distance. The tower stands out against the backdrop of the dense forest, adding a man-made element to the natural landscape.

- Lu, K., R. Zhang, X. Huang*, Y. Xie*, A Hierarchically Aligned Visual-Language Model for Enhanced Remote Sensing Image Comprehension (under review)

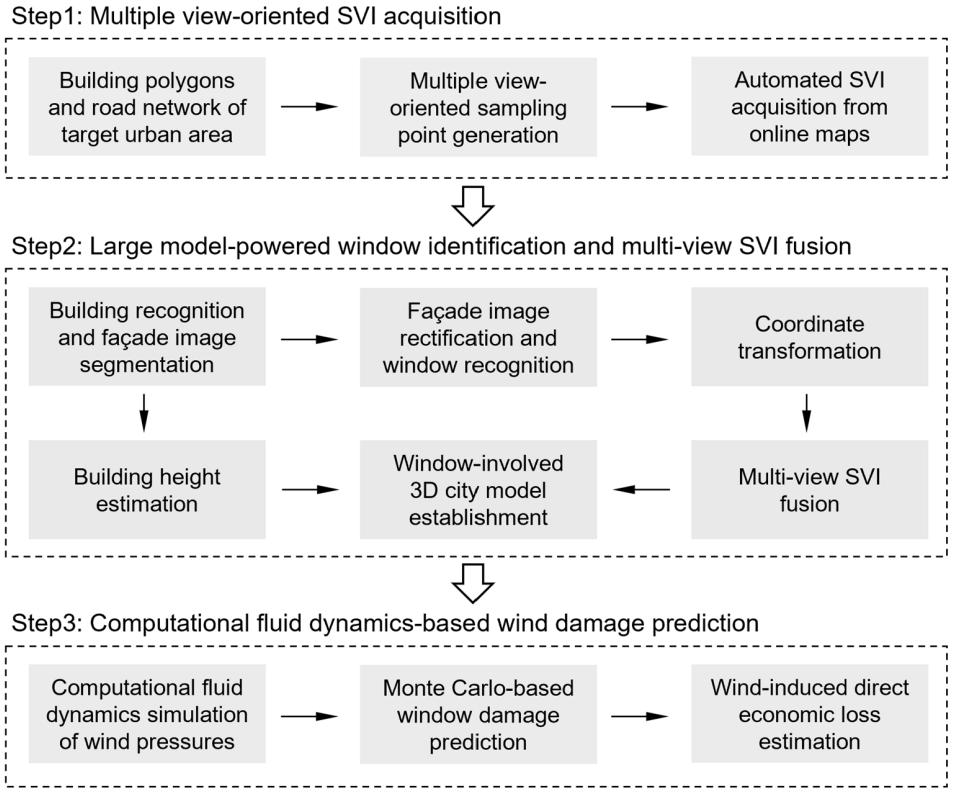
Results Reporting: Urban Sensing and Monitoring

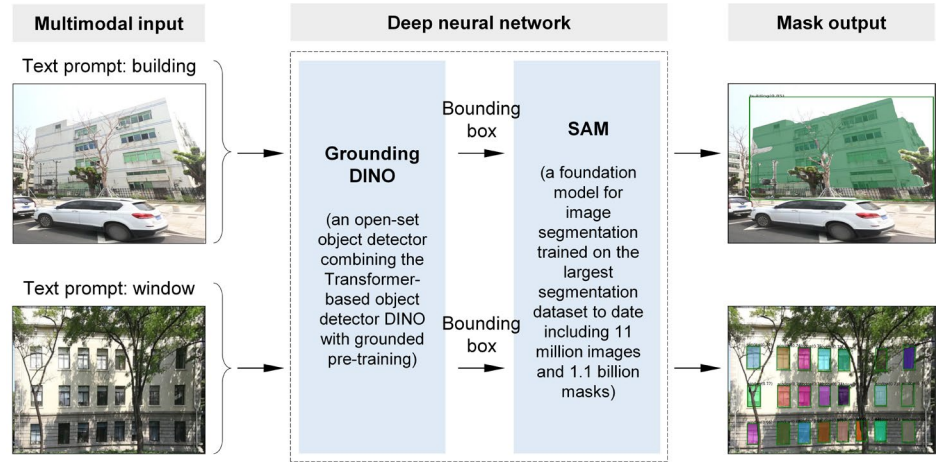
- Flood detection with SAR images (ongoing)

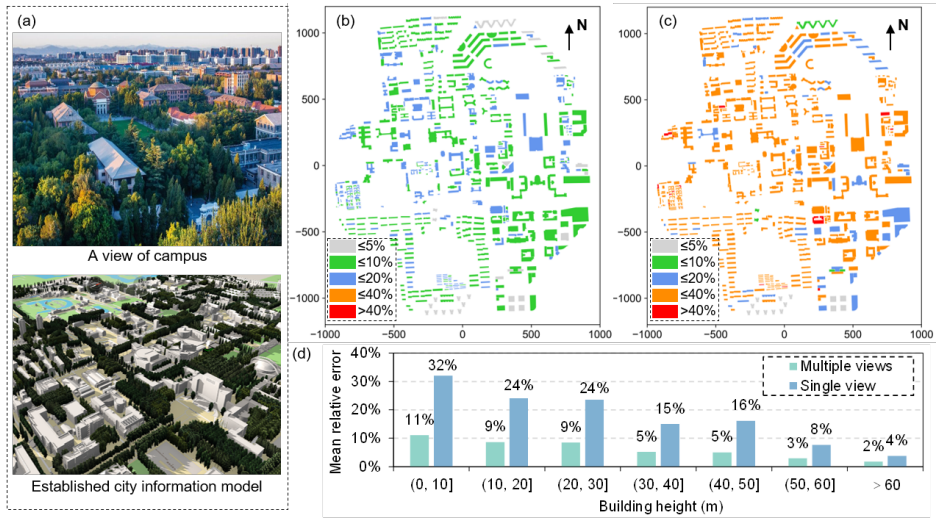


Results Reporting: Urban Disaster Simulation

- A city-scale workflow for assessing wind-induced window damage by fusing multi-view images, enabling cost-effective wind damage predictions and supporting urban resilience planning.



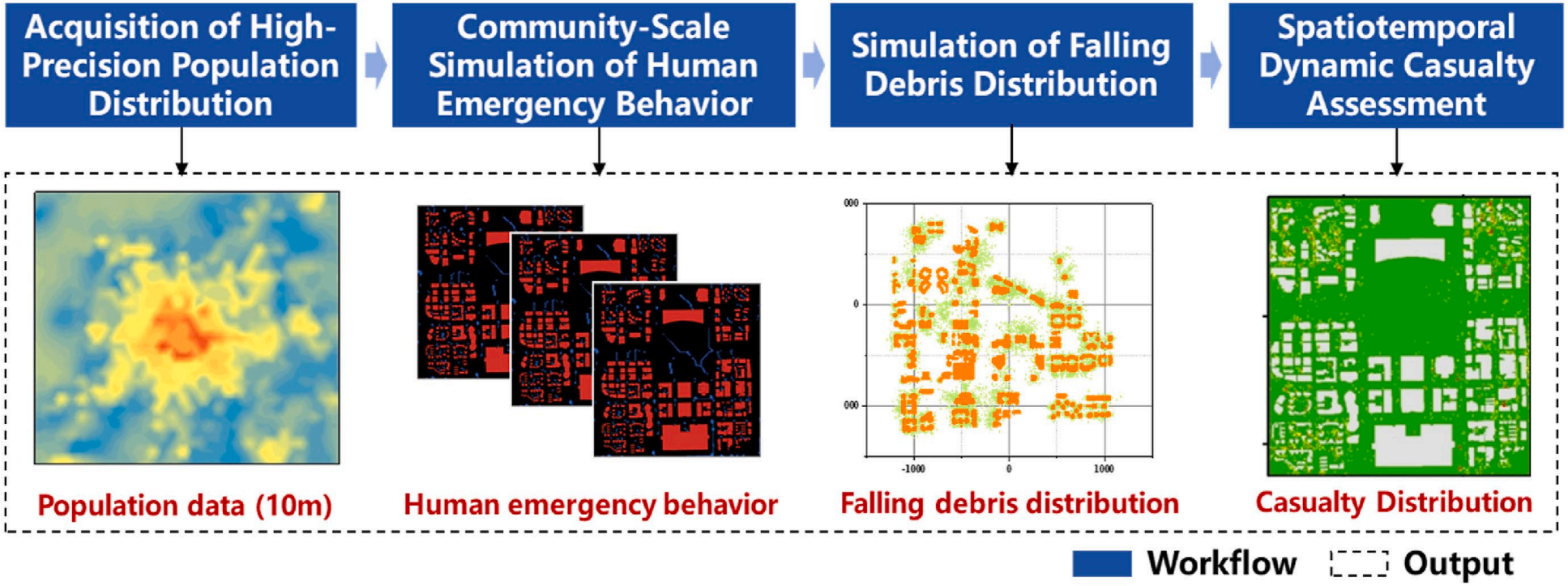




- Gu et al. (2025). Multi-View Street View Image Fusion for City-Scale Assessment of Wind Damage to Building Clusters. Computer-Aided Civil and Infrastructure Engineering, 40(2), 198–214.

Results Reporting: Urban Disaster Simulation

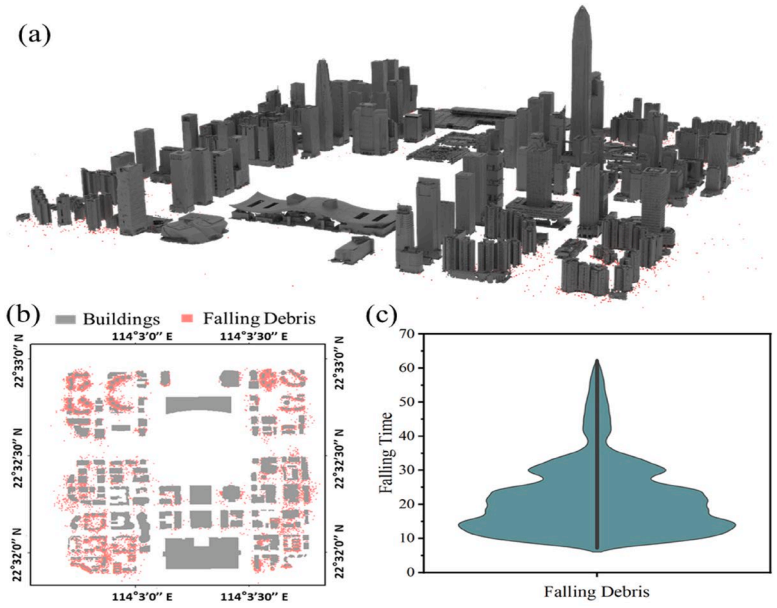
- A spatiotemporal casualty assessment method for earthquake-induced falling debris in urban building clusters, integrating building footprints, high-resolution population distribution, realistic human emergency behavior modeling, and physical debris simulations.

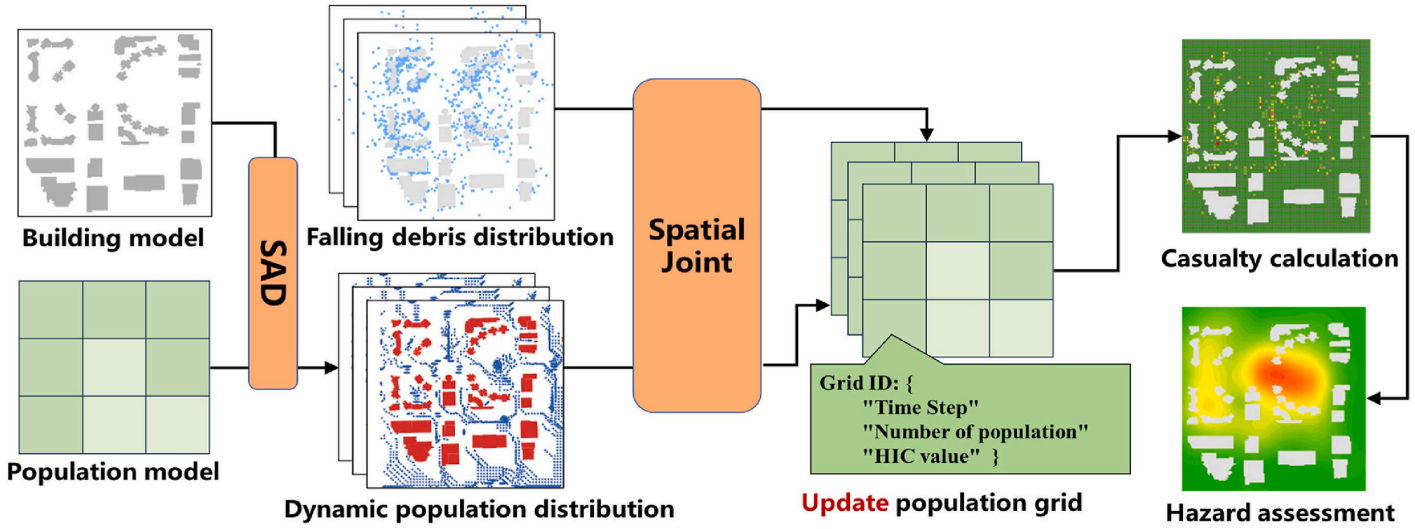


- Xu et al. (2025). A Spatiotemporal Casualty Assessment Method Caused by Earthquake Falling Debris Considering Human Emergency Behaviors. International Journal of Disaster Risk Reduction, 105206.

Results Reporting: Urban Disaster Simulation

- A spatiotemporal casualty assessment method for earthquake-induced falling debris in urban building clusters, integrating building footprints, high-resolution population distribution, realistic human emergency behavior modeling, and physical debris simulations.

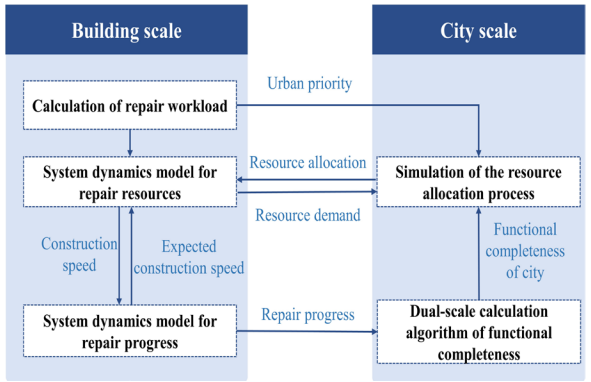




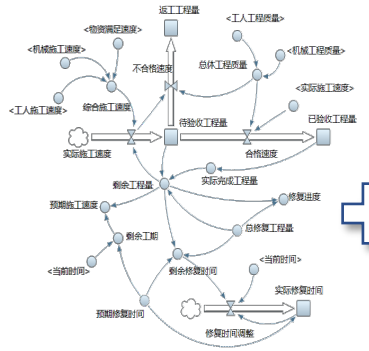
- Xu et al. (2025). A Spatiotemporal Casualty Assessment Method Caused by Earthquake Falling Debris Considering Human Emergency Behaviors. International Journal of Disaster Risk Reduction, 105206.

Results Reporting: *Beijing Resilient Urban Space Special Plan*

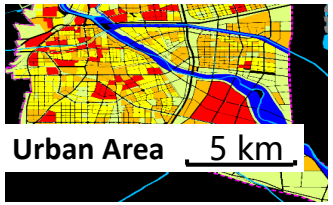
- Beyond academic contrbutions, the proposed methods have also been implimented in urban planning practices, contributing to the *Beijing Resilient Urban Space Special Plan*.



Cross-scale feedback relationships

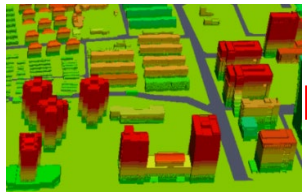


System dynamics models



GIS grid data

High-accuracy simulation



Buidling Objects





Beijing Resilient Urban Space Special Plan (2024 — 2035)

Plan for the Following Year

- Develop city-scale waterbody and flood extraction/change detection methods with optical images and/or SAR images.
- Develop disaster simulation workflows to assess urban damage caused by natural hazards (e.g., building damage, tree falling).
- Contribute to the applications of urban planning and resilience enhancement, mainly in Beijing.



CSTEC
中国科学技术交流中心
China Science and Technology Exchange Center

esa
THE EUROPEAN SPACE AGENCY

Thank you!
Questions?